Lab on a Chip

Accepted Manuscript

This article can be cited before page numbers have been issued, to do this please use: S. Rampini, P. Li and G. Lee, *Lab Chip*, 2016, DOI: 10.1039/C6LC00707D.

ROYAL SOCIETY OF CHEMISTRY

www.rsc.org/loc

View Article Online
DOI: 10.1039/C6LC00707D

Lab on a Chip

CRITICAL REVIEW

Micromagnet arrays enable precise manipulation of individual biological analyte-superparamagnetic bead complexes for separation and sensing

Received 00th January 20xx,
Accepted 00th January 20xx

DOI: 10.1039/x0xx00000x

www.rsc.org/

S. Rampini,[a] P. Li [a] and G. U. Lee [a,] *

In this article, we review lab on a chip (LOC) devices that have been developed for processing magnetically labelled biological analytes, *e.g.*, proteins, nucleic acids, viruses and cells, based on micromagnetic structures and a time-varying magnetic field. We describe the methods that have been developed for fabricating micromagnetic arrays and the bioprocessing operations that have been demonstrated using superparamagnetic (SPM) beads, *i.e.*, programmed transport, switching, separation of specific analytes, and pumping and mixing of fluids in microchannels. The primary advantage of micromagnet devices is they make it possible to develop systems that control individual SPM beads, enabling high-efficiency separation and analysis. These devices do not require hydrodynamic control and lend themselves to parallel processing of large arrays of SPM beads with modest levels of power consumption. Micromagnet devices are well suited for bioanalytical applications that require high-resolution separation, *e.g.*, detection of rare cell types such as circulating tumour cells, or biosensors applications that require multiple magnetic bioprocessing operations on a single chip.

1 Introduction

The complex nature of biomedical samples means that successful bioanalytical techniques require highly efficient separation processes, *e.g.*, isolation of rare cells from blood involves several rounds of centrifugation followed by affinity separation. For example, the separation efficiencies for circulating tumour cells (CTCs) needs to reach at least 1 part in a billion to be of use for therapeutic monitoring.[1] The separation of these bioanalytes is complicated by the fact that blood is a heterogeneous medium composed of a number of components that promote nonspecific adhesion. Thus, there is a need for new separation technologies that allow biological analytes, such as CTCs, to be isolated with a higher efficiency and analysed at a single cell level with techniques that provide quantitative information about their protein and nucleic acid properties. For example, it would be helpful if separation techniques could be developed that allow higher-efficiency recovery of cells based on the density of on or more cellular markers.

Nano- and micron-sized superparamagnetic beads functionalised with specific surface chemistries are widely used as materials to separate and detect biological analytes from complex samples, perhaps the most important tasks in bioanalytical systems.[2-5] The favourable mass transport properties, high surface area of dense suspensions of magnetic beads, and very low magnetic background of most biological samples can significantly reduce processing times and produce excellent separation efficiencies.[6] Initially, separation was focused on affinity separation of cells and other high value analytes using SPM beads functionalised with antibodies.[2] Rare cell and virus separation has been performed at efficiencies as high as a single neonatal or circulating tumour cells per millilitre of blood.[7] Ion exchange chromatography coatings have also been widely employed to extract polynucleotides from cell lysates for nucleic acid amplification testing.[8] More recently, reverse phase chromatography has been performed to isolate proteins, although the purity of the product is not as high as the other techniques.[9] Bead-based separation and assays have been integrated with automated electromagnetic systems to perform high-throughput and high-content analysis, eliminating the need for time consuming and complicated centrifugation and chromatography steps. As a result of their favourable performance characteristics, global sales of SPM beads for separation and analysis reached $53 millions in 2012 with an annual growth rate of approximately 15%.[10]

Magnetic beads lend themselves for use in miniaturised assays since they can be used to overcome the sampling limitations inherent to LOC devices, and localised magnetic forces can be easily produced that are of the same order of magnitude as the hydrodynamic forces.[11] Magnetic beads have been used in LOC devices for a range of operations, *e.g.*, transport, separation, sorting, mixing and detection of a variety of biological targets including proteins, viruses and cells. Initially, on-chip bead manipulation relied on magnetic fields and field gradients generated by bulky permanent magnets or electromagnets located beside a specific fluidic microchannel on the chip. Demonstrations reported using this strategy include DNA extraction,[12] bead

[a] School of Chemistry and Chemical Biology, UCD, Dublin, Ireland.
* Corresponding author. Tel +353 1716 2399; Fax +353 1 716 1178; e-mail, gil.lee@ucd.ie

View Article Online
DOI: 10.1039/C6LC00707D

sorting,[13] cell separation,[14, 15] rare cell isolation,[16, 17] fluidic control,[18-20] and target detection.[21-23] The simplicity of these experimental systems is certainly attractive, but the formation of SPM bead aggregates in a region of the LOC device produces biological analytes coated with a dense layer of SPM beads. These aggregates can be used to directly detect a biological analyte,[24, 25] but also severely attenuate optical signals and can lead to mechanical disruption of rare and fragile cells.

Micromagnetic features patterned inside microfluidic channels can be used to create strong magnetic field gradients, *i.e.,* between 10^4 and 10^5 T/m, in a highly localised volume.[26, 27] Figure 1 shows the most common types of microfabricated magnetic patterns, namely soft ferromagnetic elements, Figure 1a, hard magnetic elements, Figure 1b, and thin magnetic films with alternating magnetic domains separated by domain walls, Figure 1c. The combination of an external rotating magnetic field with microfabricated magnetic structures opens the possibility for a range of precise single particle operations. The micromagnet arrays have been used to transport magnetic beads and magnetically labelled analytes with nm-precision; rapidly separate multiple components in mL-scale volumes; pump and mix fluids inside microchannels without external fluidic systems; and detect magnetic beads and biological targets. The operations demonstrated to date indicate that micromagnetic arrays are a powerful new mean for the creation of LOC devices in which individual cells (and other biological analytes) can be isolated and analysed with a high degree of precision.

Electromagnets have also been microfabricated in LOC microchannels for magnetic manipulation.[28, 29] These structures are capable of producing magnetic field gradients of 10^4-10^5 T/m in localised areas, producing sufficient force for SPM bead control. Several designs have been developed for microelectromagnets, such as current–carrying microfabricated wires,[30-33] high aspect ratio trenches,[34, 35] and arrays of coils.[36] These microfabricated electromagnets have proven to be an effective solution for enabling on-chip transport and separation of SPM beads.[32, 34] Electromagnet transport of magnetically labelled cells has also been demonstrated with nanometre precision as well as the separation of viable from non–viable cells.[31] These electromagnetic microstructures do, however, introduce limitations in terms of the complexity of fabrication and the need for highly regulated power levels. This can be illustrated by estimating the dimension of a wire required for manipulating an SPM bead. Ampere's law can be used to define the magnetic field generated by a current carrying wire, *e.g.*, a 50 mA current generates a 100 Oe magnetic field. It can be shown using Preece's law that a 500 mA current has a fusing dimension of 34 μm for copper, which is a thickness that is not easily achieved using conventional microlithographic processes. The on-chip heating resulting from a large number of these electromagnets also is a limitation for the manipulation of biological samples that are sensitive to temperature.

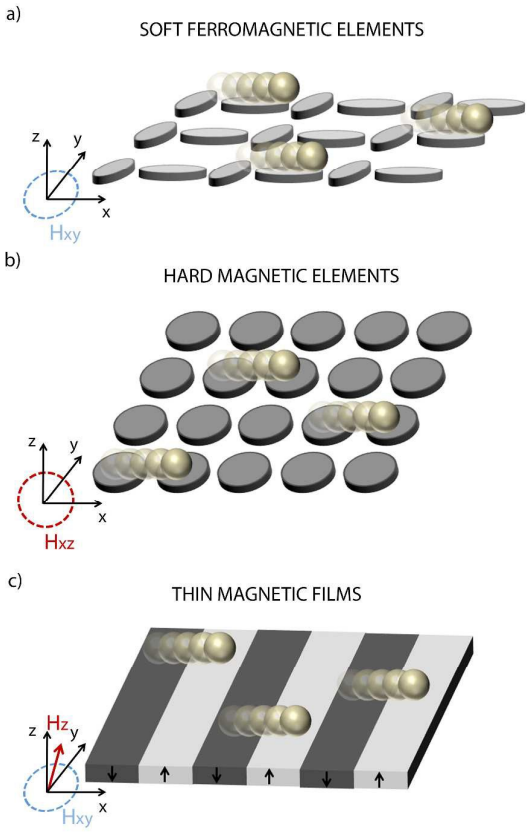

Fig. 1 Schematic representation of microfabricated magnetic structures combined with an external rotating magnetic field for superparamagnetic bead transport (grey spheres). (a) *Soft ferromagnetic elements*. The in-plane rotation of the external field modifies the magnetisation of the elements, thus transporting the beads along the perimeter of the elements in the same orientation of rotation of the field. (b) *Hard magnetic elements.* The micromagnets generate a periodic magnetic field landscape, in which the magnetic beads are trapped. The out-of-plane rotation of an applied field continuously shifts the positions of the local magnetic field maxima. (c) *Ferrite garnet magnetic films.* In these films there are oppositely oriented magnetic domains separated by domain walls. The rotation of an in-plane field modifies the size of the domains, whereas a perpendicular field determines the direction of the bead motion.

In this article, we present the first review of LOC devices based on micromagnets and rotating magnetic fields. In Section **2** the different materials that have been used to produce micromagnetic structures are introduced, *i.e.*, demagnetisable soft magnetic elements, hard ferromagnetic micromagnets, thin magnetic films with magnetic domain walls (DWs), and thin magnetic conduits of tuneable shape. Our intention is to provide a basic understanding of how different magnetic materials have been employed and the relatively advantages and disadvantages of each material. We also present a theoretical description of the motion of the SPM beads in the different micromagnet geometries. In Sections **3** to **4** we review the microfabricated magnetic structures that have been created from these materials and the resulting bioanalytical systems. Section **5** describes the manipulation of cells labelled with magnetic beads. Section **6** introduces new functionalities that have been demonstrated with micromagnet arrays, such as, bead assembly and fluid pumping.

2 Microfabricated magnetic structures

View Article Online
DOI: 10.1039/C6LC00707D

2.1 Soft ferromagnetic elements

SPM bead transport on microfabricated magnets was initially described using soft ferromagnetic elements (SFEs) composed of $Ni_{0.8}Fe_{0.2}$ with a thickness varying between 40 and 100 nm. NiFe based alloys have been extensively studied and shown to have thermal, electrical, and magnetic properties that are defined by their chemical composition and crystal structure.[37] Permalloy ($Ni_{0.8}Fe_{0.2}$) is a widely used soft magnetic material notable for its low coercivity, anisotropic magnetoresistance, and high magnetic permeability, and it has been commonly employed in MEMS for sensors and actuators, especially for applications in which currents are involved.[38, 39] Standard lithographic patterning techniques have been used to create micromagnet arrays with 1 to 10 µm scale dimensions.[40-59] These SFEs are easily de-magnetised in the presence of 5 to 15 kA/m in-plane magnetic fields (H_{xy}). Bead transport has been studied on a number of SFE designs, *i.e.*, ellipses,[40-42, 44, 51] connected disks or half-disks,[46, 53, 56, 57] disks,[47-50, 52, 54, 55, 59] triangles,[45, 55] and more complex configurations,[43, 58] using external magnetic fields created by electromagnets or by the rotation of permanent magnets.[43, 44, 50]

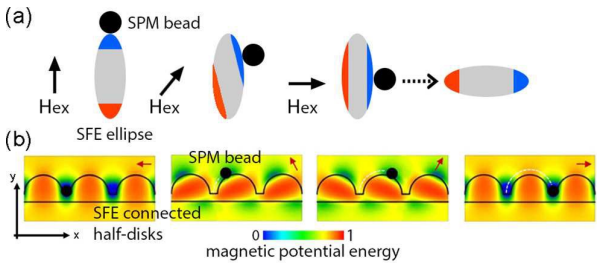

Fig. 2 Design and operation of soft ferromagnetic element arrays (a) Schematic representation of SPM bead motion along elliptical SFEs. The clockwise in-plane rotation of an applied magnetic field (H_{xy}) modifies the magnetic stray field generated by the elliptical SFEs. The SPM beads (black spheres) are trapped in the region of magnetic potential energy minima (blue) and are transported from right to left along the perimeter of the ellipses. Then the beads jump to an adjacent elliptical element arranged perpendicularly which is magnetically saturated when the external fields is perpendicular to its starting orientation. The radial forces between the two elements govern the movement of the bead from one element to the adjacent one. (b) Connected half-disk SFEs. The position of the magnetic bead (black circle) follows the local magnetic potential energy minima (blue) around the SFE as the in-plane applied magnetic field (red arrow) is rotated in a clockwise orientation, resulting in bead transport from left to right.[56] Adapted with permission.

Figures 2 presents the principle of SPM bead transport across two different SFE geometries in terms of colours that are correlated with the magnetic potential energy. Common to each of these SFE arrays is the use of a periodically rotating in-plane external magnetic field that modifies the magnetisation of the elements resulting in the transport of the beads along their perimeter. The relationship between the magnetic force, $\boldsymbol{F_m}$, exerted on the SPM beads and the magnetic field, $\boldsymbol{B}$, is defined by the equation

$$\boldsymbol{F_m} = (\boldsymbol{m}\nabla)\boldsymbol{B} = \mu_0(\boldsymbol{m}\nabla)\boldsymbol{H} = \frac{1}{2}\mu_0\chi V\nabla H^2, \quad (1)$$

where $\boldsymbol{m}$ is the bead magnetic moment, χ is the bead's magnetic susceptibility, V is the bead volume, and $\boldsymbol{H} = \boldsymbol{B}/\mu_0$ is the magnetic field strength. The linear relationship between $\boldsymbol{m}$ and $\boldsymbol{H}$ used to derive the third term in this equation ($\boldsymbol{m} = \chi V\boldsymbol{H}$) is only valid for magnetic fields that do not saturate the SPM bead, *i.e.*, less than *ca* 200 Oe, where the magnetic susceptibility is constant.[60] The term $(\boldsymbol{H}\nabla)\boldsymbol{H}$ has been rewritten in Eq. 1 as $\frac{1}{2}\nabla H^2$ by using the fact that $\boldsymbol{H}$ is curl-free inside the SPM bead. These SPM beads possess a magnetic potential energy $\boldsymbol{U_m}$

$$\boldsymbol{U_m} = -\mu_0\boldsymbol{m}\cdot\boldsymbol{H} = -\frac{1}{2}\mu_0\chi V H^2, \quad (2)$$

where **H** is the net field evaluated at the bead's centre, determined by the local field created by the magnetic elements and the external time-varying field.[61] Thus, the SPM beads are attracted to regions of maximum local magnetic field, which are also the regions of minimum magnetic potential energy.

Figure 2a presents the magnetic potential energy of elliptical SFEs as an in-plane field, H_{xy}, is rotated through three angles. As the field rotates the SPM bead (black circle) moves with the local potential energy minimum (magnetic field maximum) around the ellipse's perimeter. Magnetic saturation occurs when the external field is oriented parallel to the major axis of the ellipse, which creates a local magnetic potential energy minimum at one edge. When the field is oriented perpendicular with respect to its initial orientation (Figure 2a, right), the bead jumps to the adjacent elliptical element, which is aligned with the field and is magnetically saturated. The movement of the bead from one element to the adjacent one is governed by the radial forces between the two elements.[44] In connected half-disk SFEs, as shown in Figure 2b, the SPM beads (black circle) experience the strongest forces along the curved edge of the elements. The magnetic field maxima are determined by the orientation of the in-plane rotating magnetic field and the rotation of the applied field shifts their position, moving the beads along the SFE.[56] In the case of symmetric SFEs, such as disks, an additional out-of-plane magnetic field, H_z, is required to move the beads from one element to another; otherwise the beads simply exhibit a circular orbit.[47-49, 54] The out-of-plane field is used to weaken or strengthen the potential energy minima depending on the orientation of the local magnetic field (antiparallel or parallel) so that the beads jump from a weak trapping site of one element to the stronger trapping site of the adjacent element.[59]

2.2 Hard magnetic elements

Hard-magnetic elements (HMEs), which are capable of holding their magnetisation in an external magnetic field up to 8 kA/m, have also been extensively studied.[62-72] These permanent micromagnetic structures have been created from cobalt,[62-66] Co-Cr,[69, 71, 72] Co-Pd multilayers,[68] or alternating layers of Co and Pt.[67, 70] Cobalt based thin films have attracted much attention in magnetic applications, such as, recording media, due to its high-magnetic anisotropy, excellent coercivity, and highly chemical stability to corrosion.[73, 74] Cobalt is physically deposited between 70 and 100 nm in thickness and patterned by lift-off process in rectilinear periodic arrays,

View Article Online
DOI: 10.1039/C6LC00707D

typically formed by 5 µm circular micromagnets with 8 µm lattice periodicity. Micromagnets of larger size,[67] or different shape,[62, 63] have also been studied. The applied magnetic field rotating out-of-plane (H_{xz}) is generated by programmable electromagnets arranged along mutually orthogonal axes and supplied with sinusoidal current with a phase difference of 90°. The magnetic field strength is typically in the range 4 to 8 kA/m, giving rise to a force exerted on the beads of the order of a few tens of pN.

SPM bead transport across arrays of HMEs has been described by Yellen and co-workers.[64] Beads are trapped in the local magnetic potential energy minima that move across the array at a rate defined by the rotation of the external field (Figure 3). The local magnetic field takes the form of a travelling wave on a periodic array of HMEs. In one dimension the magnetic force applied to a SPM bead can be expressed as a function of the relative position of the beads with respect to the nearest potential energy minimum

$$F_x(x,t) = F_m sin(kx - \omega t), \quad (3)$$

where ω is the rotational frequency of the external magnetic field, $k = 2\pi/d$ describes the spatial periodicity of the array and d is the centre–to–centre distance between adjacent micromagnets. Therefore, the equation of bead motion can be expressed as

$$M\frac{d^2x}{dt^2} - \Upsilon\frac{dx}{dt} = F_m sin(\phi), \quad (4)$$

where M is the bead mass, Υ is the viscous drag coefficient of the beads, and ϕ is the phase lag between the bead position and the position of the nearest minimum, *i.e.*, $\phi = kx - \omega t$.[64] The inertia terms can been neglected due to the steady flow regime in microfluidic systems,[75] and the equation can be re-written in dimensionless form as a function of the phase ϕ

$$\frac{d\phi}{d\tau} = sin(\phi) - \frac{\omega}{\omega_c}, \quad (5)$$

where $\omega_c = F_m k/\Upsilon$ is the bead critical frequency and τ is the dimensionless time, $\tau = t\omega_c$. This equation has two characteristic solutions depending on the rotational frequency of the applied field. In the low frequencies regime ($\omega < \omega_c$) the beads travel across the magnets at an average velocity that is directly proportional to the field rotational frequency ("phase–locked" regime), *i.e.* the beads travel at the same velocity of the potential energy landscape. Above the critical frequency ($\omega > \omega_c$), the beads slip out from the potential energy minima and start undergoing a rocking motion between adjacent micromagnets ("phase–slipping" regime), thus reducing their average velocity. Therefore, the velocity profile of the beads can be described as

$$\left\langle\frac{dx}{dt}\right\rangle = \begin{cases} \omega\frac{d}{2\pi} & for\ \omega \le \omega_c \\ \left(\omega - \sqrt{\omega^2 - \omega_c^2}\right)\frac{d}{2\pi} & for\ \omega > \omega_c . \end{cases} \quad (6)$$

The critical frequency depends on the properties of the experimental configuration and on the properties of the beads. If we assume the damping results from the viscous drag, the critical frequency becomes

$$\omega_c = \frac{(\chi\,\mu_0\,\sigma_0\,H_{ext})}{18\eta}\,(2\pi\beta)^2 e^{-2\pi\beta} \quad (7)$$

where σ_0 is an experimentally determined parameter that describes the field distribution generated by the micromagnets, η is the viscosity of the medium, and $\beta = r/d$ is the ratio of the bead radius, r, to the centre to centre distance between adjacent micromagnets.[64] The critical frequency has been studied and modified to account for different approximations regarding the micromagnets' field.[65, 66]

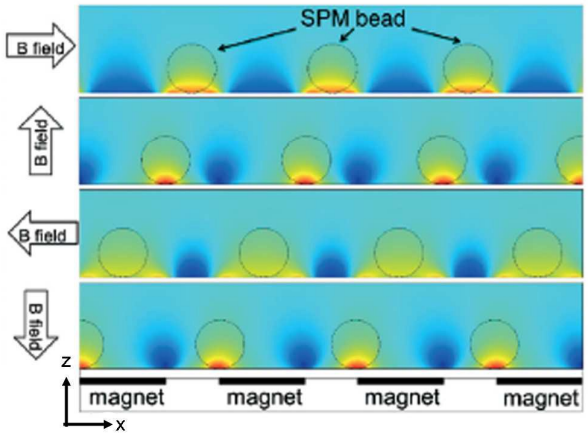

Fig. 3 Shift of magnetic field maxima in a hard magnetic array. Finite element simulations showing the local distribution of the magnetic field in a micromagnet array for different orientations of an external magnetic field rotating out-of-plane (θ_{xz} = 0°, -90°, -180°, -270°). The warm coloured areas (red) correspond to maxima of the magnetic field. The transparent circles indicate the expected locations of the SPM beads, which shift across the array from right to left, following the counter clockwise rotation of the applied field. Reprinted with permission from P. Li, A. Mahmood and G. U. Lee, Langmuir, 2011, 27, 6496-6503, Copyright 2011 American Chemical Society.[69]

2.3 Domain Wall (DW) motion in thin magnetic films and conduits

The magnetic stray field generated by magnetic domain walls in thin magnetic films has also been used to control the transport of SPM beads.[76, 77] Domain walls are narrow (~20 nm) transition regions in which the film magnetisation rotates from one orientation to a different one. The most common strategy relies on the spontaneous creation of magnetic domains in ferrite garnet films (FGF, 5 µm thick) deposited on gadolinium gallium garnets (GGG), which are compatible with substrates such as silicon and

View Article Online
DOI: 10.1039/C6LC00707D

glass. The garnet based thin films have attracted significant attention because of their applications in magneto-optics and data storage. These films can be formed by bismuth substituted ferrite garnet materials, $Y_{2.5}Bi_{0.5}Fe_{5-q}Ga_qO_{12}$,[78-90] which spontaneously magnetise in an orientation perpendicular to the plane of the film (Figure 4a). A striped pattern of upward and downward domains (periodicity $\lambda \sim 2w \sim$ 10 μm) can be observed in these films via polarised light microscopy due to the Faraday effect. A "bubble" domain lattice can be created by applying high frequency (10 kHz) magnetic field pulses ($\sim 3M_s$, with M_s saturation magnetisation of the film) perpendicular to the film (along the *z*-axis in Figure 4b).[80-84, 88] The "bubbles" are cylindrical domains of reverse magnetisation (diameter ~8 μm) separated by a continuously magnetised film. Alternatively, DWs have been artificially created in exchange biased magnetic bilayers.[91-93] DWs have been created in $Si/Ta^{5.3nm}/Ru^{2.03nm}/Ir_{17}\ Mn_{83}^{11.6nm}/N_{i80}Fe_{20}^{7.75nm}/Ta^{3.6nm}$ bilayer systems via ion-bombardment, producing a pattern of stripes with opposite in-plane magnetisation.

The local magnetic stray field generated by a DW acting on a magnetic bead can be expressed as

$$\boldsymbol{H_{DW}} = \left(\frac{\boldsymbol{M_s w}}{\boldsymbol{2\pi r}}\right)\left(\frac{\boldsymbol{\rho}}{|\boldsymbol{\rho}|^2}\right), \quad (8)$$

where $\boldsymbol{\rho}$ is a vector pointing from the DW to the bead, *w* is the wall width and *r* is the bead radius.[76, 77] The applied magnetic field ranges between 10^3 and $5x10^4$ A/m, giving rise to forces in the pN range.

Bead motion is controlled with a magnetic field rotating out-of-plane, inclined by an angle θ with respect to the *z*–axis. The bead transport mechanism is illustrated in Figure 4a. The SPM beads are captured by the local stray field generated by the DWs (Figure 4a-i). The size of the magnetic domains is determined by the component of the applied magnetic field perpendicular to the film, H_z, as shown in Figure 4a-ii. The beads hop from one DW to the adjacent one due to the effect of the in-plane component of the external magnetic field, H_{xy} which alters the strength of the pinning sites at the walls. The orientation θ determines the direction of bead motion. In case of a "bubble" domain lattice, as shown in Figure 4b, an in-plane field H_{xy} is applied in combination with a perpendicular field component, H_z, to control the bead transport in two dimensions. In exchange biased magnetic bilayers the transport mechanism is slightly different, *i.e.*, it is controlled by magnetic field pulses applied along the *x*-and *z*- directions.

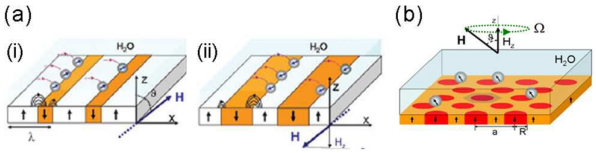

Fig. 4 DW guided motion of SPM beads across thin magnetic ferrite garnet films (FGFs). (a) The magnetic domains in the film form a striped pattern of oppositely oriented domains (white and orange stripes). An applied out-of-plane rotating field (H_z) shifts the position of the beads (white circles) across the surface by varying the size of the magnetic domains, depending on their orientation with respect to the external field. An in-plane field (H_{xy}) changes the strength of the pinning sites, thus making the beads hop from one domain to the adjacent one. Reproduced from Ref. [84] with permission from The Royal Society of Chemistry. (b) Magnetic "bubble" domain pattern formed in a thin magnetic film due to applied high frequency magnetic field pulses. The red and orange areas correspond to magnetic domains of opposite orientation. The out-of-plane rotation of a magnetic field, tilted by a positive (negative) angle with respect to the *z*-axis, determines the transport of the beads (white spheres) in the forward (backward) direction. Reprinted with permission from P. Tierno, S. V. Reddy, J. Yuan, T. H. Johansen and T. M. Fischer, The Journal of Physical Chemistry B, 2007, 111, 13479-13482, Copyright 2007 American Chemical Society.[79]

A slightly different approach relies on the motion of DWs constrained in thin ferromagnetic conduits.[94, 95] These magnetic elements have been fabricated from $Fe_{0.5}Co_{0.5}$ (M_s ~2 T),[47, 59, 96-100] Ni,[101] or NiFe,[102-111] in shapes that included zig-zag wires,[47, 59, 96, 97, 100, 102-106] rings,[101, 103, 104, 107-109] squares,[104] straight wires with periodic indentations,[98] and curvilinear tracks.[110] Examples of conduits patterned on polymeric[105] or piezoelectric substrates,[101] have also been reported. The thickness of the structures is commonly between 13.5 and 40 nm with a width of as little as a few 100 nms. After the fabrication process, the thin conduits are saturated with an in-plane magnetic field on the order of 80 kA/m. For zig-zag nanowires, the applied field generates a distribution of consecutive head-head (HH) and tail-tail (TT) magnetic domains located at the vertices of the wire (Figure 5a).[98] In ring conduits the applied saturating field generates two magnetic domains separated by one HH and one TT domain walls ("onion state", Figure 5b).[103] The constrained DWs generate a magnetic stray field with radial distribution directed outwards the DW (+*z*-direction) in the case of a HH domain, or directed inwards in the case of a TT domain (-*z*-direction). Due to the dependence of the magnetic force on the gradient of the field squared, both HH and TT domain walls generate an attractive force on SPM beads, which is on the order of 10 pNs. The bead transport on these structures is governed with two magnetic fields applied in the *xy*-plane, H_{xy}, and along the z-direction, H_z. The applied magnetic field strength is usually between 8 and 16 kA/m. The field H_z can change the nature of the trapping sites from attractive to repulsive, depending on its relative orientation with respect to the local field generated by the DW. The in-plane field H_{xy} drives the DWs and the SPM beads pinned to the DWs along the nanowires or along the perimeter of the ring structures in the direction of the field orientation. An alternative approach to control the DW motion is based on the induced strain in a piezoelectric film on which the conduits are patterned.[101]

View Article Online
DOI: 10.1039/C6LC00707D

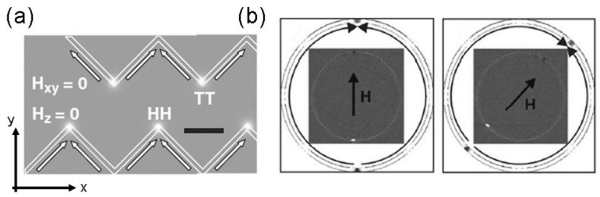

Fig. 5 Constrained domain walls in thin magnetic conduits. (a) In zig-zag nanowires the magnetic domains are separated by consecutive HH and TT domain walls that create trapping sites for the SPM beads at the vertices of the wires. The in-plane rotation of an applied magnetic field shifts the locations of the magnetic field maxima along the wire, thus transporting the beads along the conduit. Reprinted with permission from G. Vieira, A. Chen, T. Henighan, J. Lucy, F. Yang and R. Sooryakumar, Physical Review B, 2012, 85, 174440 Copyright 2012 by the American Physical Society.[98] (b) In ring structures, two magnetic domains are formed that are separated by a HH and a TT domain walls ("onion-like" state). The in-plane rotation of the magnetic field shifts the domain walls along the perimeter of the conduit, thus transporting the SPM beads (grey spheres).[103] Reproduced with permission.

2.5 Summary

Table 1 summarises the magnetic and physical properties of the materials presented in this section and their applications. Each of these materials has been used in a similar range of bioprocesses, *e.g.*, transport and separation, although the manner in which this can be achieved differs significantly. Saturation magnetisation is perhaps the most important property of a material since it affects the distribution and intensity of local magnetic forces. Permalloy thin films have a saturation magnetisation that is about 1000 emu/cm^3,[37, 112, 113] and hard magnetic films have a saturation magnetisation similar to that of permalloy.[73, 114, 115] The saturation magnetisation of these materials is about one order of magnitude smaller for garnet based magnetic thin films.[116-119] The equation for the critical frequency, Eqn. 7, indicates that it is linearly related to the local magnetic field generated by the micromagnet, $\boldsymbol{\sigma_0}$. This provides the SFE and HME arrays with a higher critical frequency resulting in higher velocities at which the SPM beads can be transported and separated. Advantage of HMEs is that they retain their magnetisation in the absence of external field and thus can be used to capture SPM beads without consuming power.

Micromagnetic arrays have been produced from the three different materials using well-established processes, such as photolithography, with similar size critical dimensions, in the range from 1 to 10 µm. Well-established metal deposition processes, such as, sputtering or vapour deposition techniques, have been used to produce the SME and HME micromagnet arrays. The creation of thin ferrite garnet films is a more complex process requiring dipping liquid phase epitaxy, which involves high temperatures and precise control over the deposition conditions, to control the formation of the magnetic domains.

3 Transport and separation on micromagnets

The combination of time-varying magnetic fields and microfabricated magnetic patterns permits precision positioning of SPM beads and magnetically labelled biological targets. The high precision of this strategy makes it attractive for manipulating biological targets, such as, proteins, viruses and cells, and for performing high-resolution separation. The different separation strategies that have been implemented for the structures presented in the previous section will be described here, including separation based on the bead critical frequency, multi-frequency driven systems, and engineered microstructures.

3.1 Magnetic transport

The transport of SPM beads with de-magnetisable structures was first demonstrated by Gunnarsson, *et al*. with SFE ellipses (2 µm x 6 µm x 0.1 µm) arranged in a staircase pattern (Figure 6a).[40] The in–plane rotating magnetic field determined the distortion, annihilation and nucleation of the magnetic domains inside the ellipses.[41] The beads followed the net magnetisation of the magnetic structures and were transported along the perimeter of the ellipses in the rotational direction of the field, jumping from one ellipse to the adjacent one when it became magnetically saturated (Figure 6a). A limitation to this approach was that the bead transport could only be performed in one direction. The same group also reported the transport of proteins across lines of triangular magnetic structures (6 µm x 0.07 µm).[45] Four proteins, *i.e.*, a-

Structure	Mat.	M_s	Coercivity	Common shapes	Appl. Field	Maximum Force	Applications	Ref.
De-magnetisable	NiFe	~ 1000 Oe	0.01 – 1 Oe	Ellipses, Connected half-disks	H_{xy}	1-10 pN	Transport, pumping, mixing, and separation	37-59, 112, 113
Permanent micromagnets	Co, CoCr	~ 1000 Oe	10 – 900 Oe	Disks	H_{xz}	10 pN	Transport, separation, and assembly	62-74, 114, 115
DWs in thin films	FGFs	< 100 Oe	~ 100 Oe	Stripe, "bubble" patterns	H_z, H_{xy}	1 pN	Transport, separation, mixing, and assembly	76-93, 116-119
DWs in thin conduits	FeCo, NiFe			Zig-zag wires, rings	H_z, H_{xy}	10 pN	Transport and assembly	47, 59, 94-111

Table 1 Summary of the strategies for SPM bead control with rotating magnetic fields and microfabricated magnetic elements.

View Article Online
DOI: 10.1039/C6LC00707D

lactalbumin, lysozyme, HSA and IgG (Human) were captured by functionalised SPM beads and transported at a velocity up to 20 µm/s. These proteins were detected on the immobilised beads on the magnetic structures with a fluorescently labelled secondary antibody. Thus, the authors demonstrated the potential of this technique for the capture and direct analysis of biological analytes on-chip.

Lim, *et al.* demonstrated the transport of SPM single beads and bead chains along elliptical patterned pathways (9 µm x 4 µm x 0.1 µm).[51] The authors used the chain transport as a proof of concept for the application of this approach to biological experiments, such as, the dislocation of molecules with high aspect ratio, or of magnetic beads-biological target sandwiches. A wide range of curved structure geometries was proposed by Conroy, *et al*. (Figure 6b).[43] Using a saw-tooth pattern, the authors trapped 8 µm SPM beads functionalised with goat antibodies. The beads were then transported back and forth through different flow streams to capture a complementary fluorescent antibody and then release it in an elution buffer. Therefore, the beads were used as mobile substrate for capturing an analyte suspended in a flowing solution that was subsequently released from the bead surface.

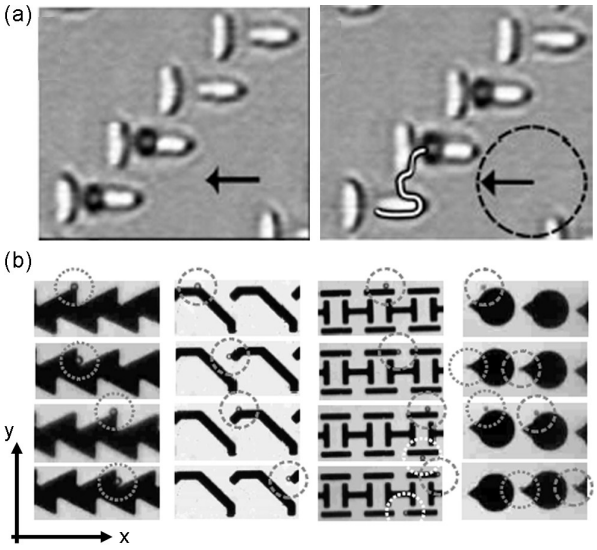

Fig. 6 Bead transport in SFEs arrays (a) Transport of SPM beads in elliptical magnetic structures. The beads travelled along the perimeter of the ellipses in the same sense of rotation of the in-plane magnetic field (counter clockwise), and jumped to an adjacent ellipse when it became magnetically saturated by the external field, *i.e.*, when the field was aligned with the easy magnetisation axis of the ellipse.[40] Reproduced with permission (b) Transport of SPM beads in a range of different curved geometries. The SPM beads moved along the perimeter of the patterned features following the in-plane rotation of the applied magnetic field. Reprinted from R. S. Conroy, G. Zabow, J. Moreland and A. P. Koretsky, Applied Physics Letters, 2008, 93, 203901, with the permission of AIP Publishing.[43]

3.2 Nonlinear Magnetophoresis (NLM)

A significant contribution to this field resulted from a series of experimental and theoretical studies on the behaviour of magnetic beads on hard micromagnet arrays.[64-67] The transport of SPM beads was achieved with the combination of an out–of–plane rotating field and an array of circular micromagnets, which generated a travelling magnetic field wave. The directionality of the bead motion was controlled by the sense of rotation of the applied magnetic field. The SPM bead velocity increased linearly with the rotational frequency of the applied field until a critical frequency (ω_c) was reached, above which the bead average velocity started reducing, as introduced in Section **2.2**. The dependence of ω_c on the bead physical properties produced a high-resolution separation process referred to as nonlinear magnetophoresis (NLM). Different bead types were separated from each other by applying a rotating magnetic field at a frequency ω at which the beads had different mobility, *i.e.*, $\omega_{(c,1)} > \omega > \omega_{(c,2)}$ (Figure 7a). The principle was demonstrated by efficiently separating low ω_c 1 µm beads from high ω_c 2.8 µm beads.[64] The authors also demonstrated the separation of unreacted beads from bead–cell complexes, *i.e.*, 1 µm beads were used to capture *B. globigii* cells, and 2.8 µm beads were used to capture *S. cerevisiae* cells. The presence of the biological target increased the hydrodynamic radius of the beads, thus reducing the critical frequency and enabling NLM separation (Figure 7b). It was possible to separate all the bead populations in a heterogeneous sample by sequentially scanning the driving rotational frequency from high to low, thus enabling multiplex separation. However, the separation efficiency was limited by the interactions that occurred between beads travelling at different velocities. The beads were immobilised on the micromagnets at the so-called "immobilisation" frequency, ω_i. The ideal scenario would be $\omega_i / \omega_c = 1$, *i.e.*, a sharp transaction from "mobile" to "immobile" beads, which would correspond to a nearly infinite resolution of the separation process. The parameter $\beta = r/d$ influenced the sharpness of the transaction.[65, 66] For low values of β (0.10–0.15) the ratio ω_i / ω_c approached unity, whereas for increased values of β, the ratio ω_i / ω_c approached a limiting value determined by the properties of the system. Fine-tuning of the micromagnet dimensions relative to that of the SPM beads increased the efficiency of the separation process. Critical frequency-based separation of 2.8 µm SPM beads from 1 µm SPM beads, was demonstrated also by Donolato, *et al.* in patterned magnetic stripes in exchange biased magnetic bilayers.[120] In this experimental design the beads experienced a magnetic force that did not vary in the *y*-direction, thus reducing the bead clustering due to magnetic interactions.

View Article Online
DOI: 10.1039/C6LC00707D

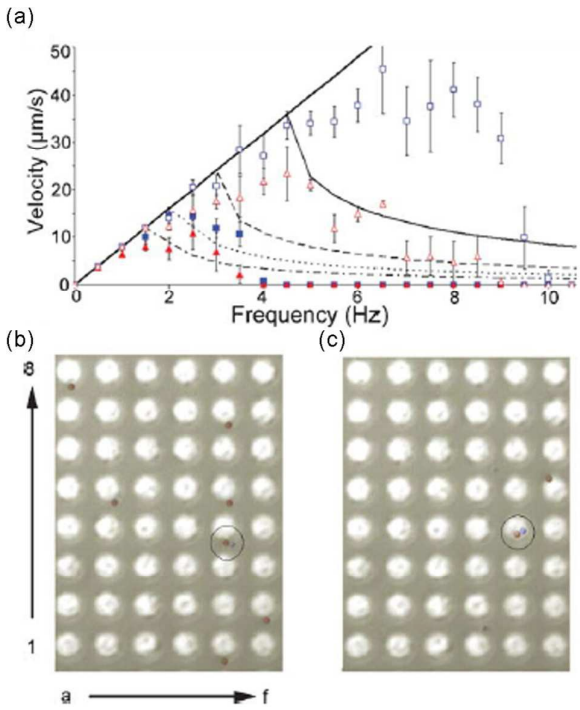

Fig. 7 Nonlinear magnetophoresis and SPM bead transport across circular micromagnet array (a) Velocity profile of different SPM bead types: 1 μm (empty triangles) and 2.8 μm (empty squares) beads, 1 μm bead-*B. globigii* complexes (full triangles) and 2.8 μm bead-*S. cerevisiae* complexes (full squares). The bead velocity increased linearly with the rotational frequency of the applied out-of-plane field , until a critical frequency was reached, above which the bead velocity decreased. The larger beads had a higher critical frequency, whereas the presence of the biological target reduced the bead critical frequency, thus allowing to separate different bead populations. (b-c) Separation of a bead-*B. globigii* complex from unreacted 1 μm beads in circular micromagnets. The bead-target complexes had lower critical frequency with respect to the bare beads, which thus could travel freely across the array while the bead-target complexes were immobilised by selecting the external magnetic field frequency. Reproduced from Ref. [64] with permission from The Royal Society of Chemistry.

3.2 Flow-enhanced magnetophoretic NLM separation

In flow-enhanced nonlinear magnetophoresis (F-NLM) micromagnetic bead separation was combined with hydrodynamic flow to enhance processing speed and efficiency of separation of different bead populations.[69, 71] Figure 8 presents results in which the hydrodynamic (*y*–direction) and magnetic (*x*–direction) forces were balanced so that 1 μm diameter beads were immobilised on the micromagnets, while 2.8 μm diameter beads were collected and separated at the edge of the micromagnet array. F-NLM was also used for the separation of SPM beads with different magnetic susceptibility between χ = 0.02 and 0.17, *i.e*, ω_c increases for increasing χ.[71] The critical frequency was found to be related to the physical properties of captured biological targets

$$\boldsymbol{\omega_c} \propto \frac{\boldsymbol{r}}{\boldsymbol{a}}, \qquad (9)$$

where *a* is the effective hydrodynamic radius of the non-magnetic target – SPM bead complex and *r* is the bead radius. The capture of a biological target on an SPM bead resulted in a decrease in the critical frequency of the complex. The correction factor in Eq. 9 quantitatively predicted the decrease in critical frequency of captured cells (*i.e*., *B. globigii* and *S. cerevisiae*),[64] and exosomes (*i.e.,* extracellular organelles that contain RNA captured with 2.8 μm beads).[71] The authors also observed the formation of bead chains on the micromagnets as a function of magnetic properties. For beads with low susceptibilities (χ < 1) the field generated by the micromagnets dominated the bead–bead interactions thus inhibiting the formation of chains. However, when χ > 1 the interactions between adjacent beads overcame the local magnetic field leading to the creation of bead chains.

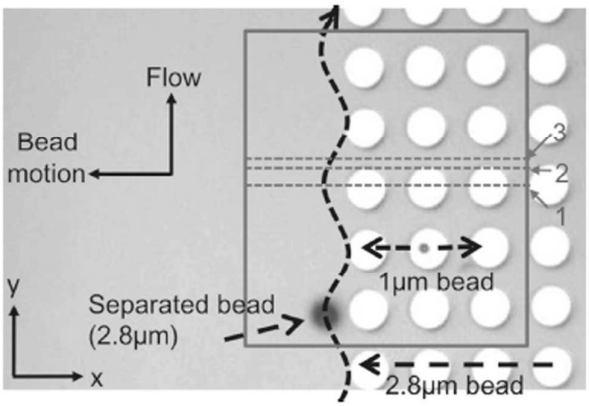

Fig. 8 F-NLM separation of SPM beads across a micromagnet array. The rotational frequencies of the external out-of-plane field, H_{xz}, were selected so smaller beads (1 μm) were immobilised on the surface, while the larger beads (2.8 μm) were free to move due to their higher critical frequency. When these beads reached the end of the array they were guided by an applied hydrodynamic flow along the *y*-direction, thus improving the separation efficiency of the two bead types. Reproduced from Ref. [69] with permission from The Royal Society of Chemistry.

3.4 Transport in which magnetisation, external magnetic field or array elements are not aligned

The examples reported in the previous two sections have presented systems in which the SPM beads travel along straight lines aligned with the magnetisation of the micromagnets. Transport has also been studied on micromagnetic arrays in which the external magnetic field was not aligned with the magnetisation of the micromagnets or the magnet arrays were not rectilinear. These systems have been used to implement novel separation and collection schemes.

The influence of magnetisation and external driving frequency has been studied for beads moving on HME rectilinear micromagnet arrays. It has been observed that beads move at an angle θ^*, relative to a micromagnet arrays' magnetisation, by applying an external rotating field at an orientation θ relative to the micromagnets' magnetisation (Figure 9a).[68] For low θ the beads tended to follow the direction of the micromagnets' magnetisation ($\theta^* < \theta$), whereas for high ϑ the beads travelled along an orthogonal trajectory ($\theta^* > \theta$). The threshold angle at which the beads switched

View Article Online
DOI: 10.1039/C6LC00707D

from $\theta^* < \theta$ to $\theta^* > \theta$ depended on their properties, such as, the size or the presence of a captured molecule that increased the viscous drag coefficient. Larger beads moved along the magnetisation track at higher driving angles than smaller beads. Therefore, it is theoretically possible to achieve 2D separation of different bead types by sequentially adjusting the driving angle θ.

Figure 9b presents a SFE micromagnet structure that has tilted bead trajectories. Obliquely arranged elliptical[44] and halfdisk[46] SFEs were used to create converging transport lines that directed the beads towards specific locations of the chip, *i.e.,* towards a sensing area that could be functionalised with specific receptors to capture the beads carrying a target analyte. The sense of rotation of the applied magnetic field was used to control the direction of bead motion, so that the SPM beads were made to converge or diverge from the sensing area. In another study, HME micromagnets were arranged in a dense converging array (Figure 9c) to focus the beads in a specific region.[72] The beads were dispensed on a rectilinear array of circular magnets, and were then transported along the converging lines that focused at a central line of micromagnets. This design proved useful in collecting large bead populations for analysis with a single point optical detector. In the same work, the authors also presented a tree-like structure in which the focusing process took place through a series of focusing junctions. The two designs were characterised with a focusing efficiency of 94.3 ± 2.9% and 89.4 ± 2.9%, respectively.

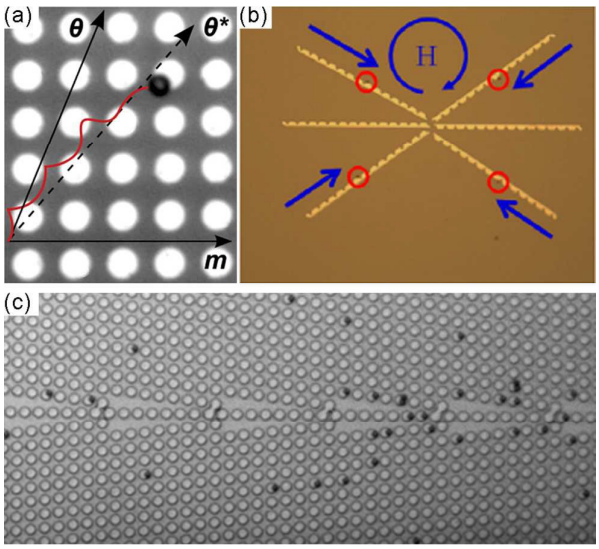

Fig. 9 Oblique transport (a) Tilted SPM bead transport across circular micromagnets. By applying an external out-of-plane rotating field at an angle θ relative to the magnetisation of the micromagnets, the bead trajectory was tilted into an angle θ^*. Separation of different bead types was achieved by selecting a tilting angle higher or lower than θ depending on the bead properties. Reprinted with permission from M. A. Tahir, L. Gao, L. N. Virgin and B. B. Yellen, Phys Rev E, 2011, 84, Copyright 2011 by the American Physical Society.[68] (b) SPM bead transport along semi-elliptical SFE converging pathways. The clockwise rotation of the in-plane applied field made the beads travelling around the pathway perimeter and converging towards a specific location. The counter clockwise rotation of the applied field transported the beads away. Reprinted from S. Anandakumar, V. Sudha Rani, J. R. Jeong, C. Kim, K. W. Kim and B. P. Rao, Journal of Applied Physics, 2009, 105, 07B312, with the permission of AIP Publishing.[44] (c) Dense array of tilted lines of HME circular micromagnets. The out-of-plane rotating field transported the beads along the *x*-direction. During their motion, the beads converged towards the centre of the chip following the micromagnet lines. Once the beads reached the centre of the array, they continued travelling along the central line of micromagnets. Reproduced from Ref. [72] with permission from The Royal Society of Chemistry.

3.5 Domain Wall magnetophoretic transport

SPM bead transport across thin magnetic films via DW motion has been investigated by Tierno and co-workers.[78-90] In thin ferrite garnet films, the magnetic domains assumed a stripe–patterned configuration with periodicity λ (~10 μm), and the SPM beads travelled a distance λ for each rotational period of the applied rotating magnetic field, so that the bead velocity was $v = \lambda\omega/2\pi$ (Figure 10a). Depending on the rotational frequency of the applied field the beads exhibited different transport regimes similarly to the NLM process described in the previous section. At low driving frequencies the beads travelled synchronously with the DW; for increasing rotational frequency the beads de-synchronised with the traveling field, and their average velocity decreased until they were immobilised on the surface.[86, 89] By tuning the applied field it was possible to induce dipolar interactions that created bead chains.[89] This transport strategy has been successfully applied to manipulating oil droplets attached to magnetic nanoparticles,[79] as a model for the application of these materials for bioassays.

By applying high frequency magnetic field pulses it was possible to create metastable "bubble" domains in the thin magnetic films (Figure 10b). [80-84, 88] The bubbles assembled in a hexagonal lattice and trapped the SPM beads along their perimeter. The size of the bubble domains increased (decreased) if a magnetic field H_z was applied that had orientation parallel (antiparallel) to the magnetic domains. If a rotating magnetic field was tilted by an angle θ with respect to the *z*-axis (Figure 4), the magnitude of the normal field component H_z could be used to determine the transport regime of the beads (keeping the frequency and the magnitude of H_{xy} constant). At low fields, the beads exhibited a closed orbit around one bubble domain at a velocity equal to the rotational frequency of the applied field (Figure 10b-i). Increasing the magnetic field *z*-component reduced the size of the bubble domains and the beads started travelling across the film, jumping from one bubble to the adjacent one (Figure 10b-ii). For even higher field magnitudes, *i.e.* lower θ, the beads experienced a triangular closed orbit between three bubble domains (Figure 10b-iii). The beads were directed along any one of the six crystallographic directions of the bubble lattice. The bead dynamics also depended on the rotational frequency and ellipticity of the applied field.[82, 83]

The transport of beads and magnetically labelled molecules using DWs has been largely studied on patterned zig-zag nanowires with HH and TT domains created at the vertices of the wire (see Section **2.2**).[47, 59, 96, 97, 102-105, 120] The DWs were shifted by applied H_{xy} and H_z magnetic fields that transported the beads along the wire (Figure 10c). The out-of-plane field, H_z, was used to control the depth of the potential energy wells located at the vertices of the wire, in which the beads were trapped, thus switching the nature of the traps from attractive to repulsive. When the amplitude of the energy wells was reduced, the SPM beads were displaced from the vertices due to the increased relevance of Brownian fluctuations. Therefore, the wires were used as tuneable magnetic traps for

View Article Online
DOI: 10.1039/C6LC00707D

capturing and releasing magnetic beads and labelled molecules, such as, DNA as demonstrated by Chen, *et al.* [59, 97]

The sequential switching of the attractive/repulsive nature of the zig-zag vertices has also been used to move the beads from one zig-zag line to the adjacent top or bottom line, demonstrating that the bead trajectory was not limited to a single pathway.[96] Demonstrations with this particular geometry include the transport of polymer micelles[47] and proteins.[103] The polymer micelles were a versatile container for the transport of nm-sized targets; in the reported example nm-sized magnetic beads were encapsulated in the micelle together with quantum dots to enable fluorescence detection. Proteins were transported along zig-zag wires with sub-µm precision in two different configurations, *i.e.*, proteins were captured by single SPM beads or by different SPM bead types that interacted to form bead doublets.

The geometry of DW conduits was not limited to a zig-zag wire configuration, and included square or ring conduits in which the DWs were smoothly and continuously shifted along the perimeter by a small applied field (H_{xy}).[101, 103, 104, 107-109] Rapoport, *et al.* reported the transport of SPM beads around the perimeter of circular DW conduits (10 µm outer diameter, Figure 10d) at a velocity up to 1000 µm/s.[107-110] Below a critical threshold rotational frequency of the applied field, the beads were transported at the same velocity of the DW. As expected, a threshold velocity of the DW was observed at higher frequencies due to the increased viscous drag. Smaller beads (1 µm) exhibited a higher critical frequency than larger beads (2.8 µm) due to the lower hydrodynamic drag, opposite to what observed for the transport across permanent micromagnets. In the same work, the authors presented the bi-directional transport of SPM beads along a curvilinear track structure, achieving a maximum average velocity of *ca.* 150 µm/s. The composition of the curvilinear structure was modified in another work to include embedded electrical sensors, thus enabling on-chip detection while preserving the magnetic transport capabilities.[108] A rectilinear array of ring DW conduits has also been proposed by Anandakumar, *et al.*.[111] An in-plane magnetic field, H_{xy}, was used to rotate the position of the SPM beads around the perimeter of the conduits, whereas a perpendicular field H_z tuned the strength of the trapping sites, thus allowing the beads to hop from one ring conduit to the adjacent one. The trajectory of the beads could thus be precisely controlled along the *x* and the *y*-directions, enabling programmable 2D transport.

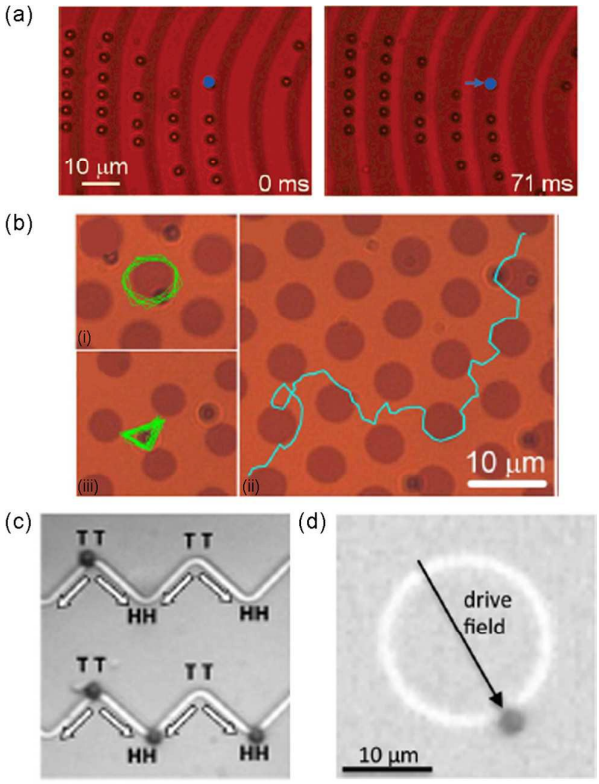

Fig. 10 DW-based transport in thin films and conduits (a) DW-guided motion of SPM beads in thin magnetic films. The magnetic domains in the film formed a stripe pattern of oppositely oriented domains (light and dark stripes). An applied rotating field (H_z) made the domains larger (smaller) depending on their orientation with respect to the field direction, *i.e.* parallel (antiparallel). The domain size variation determined the shift of the bead position across the surface, and their jumping from one domain to the adjacent one due to the effect of an in-plane magnetic field. Reprinted with permission from P. Tierno, S. V. Reddy, J. Yuan, T. H. Johansen and T. M. Fischer, The Journal of Physical Chemistry B, 2007, 111, 13479-13482, Copyright 2007 American Chemical Society. [78] (b) Trajectories of paramagnetic beads in a bubble domain lattice. The light and dark regions correspond to oppositely oriented magnetic domains. The size of the bubble domains increased (decreased) if a magnetic field H_z was applied that had orientation parallel (antiparallel) to the magnetic domains, whereas an in-plane rotating field determined the bead motion: (i) for low externally applied magnetic fields (H_z) the beads were trapped around the bubble domains, (ii) for increasing fields, the size of the bubble reduced and the beads jumped from one domain to the adjacent one (iii) at high applied fields the beads exhibited a closed orbit around three magnetic domains. Reprinted with permission from P. Tierno, T. H. Johansen and T. M. Fischer, Physical review letters, 2007, 99, 038303, Copyright 2007 by the American Physical Society. [80] (c) Zig-zag wire in which the DW formed at the vertices, and created regions of localised high magnetic field gradient that trapped the SPM beads. An in-plane rotating magnetic field shifted the DW positions along the conduit, thus transporting the SPM beads. Reprinted with permission from G. Vieira, T. Henighan, A. Chen, A. Hauser, F. Yang, J. Chalmers and R. Sooryakumar, Physical review letters, 2009, 103, 128101, Copyright 2009 by the American Physical Society. [96] (d) Circular conduit in which two opposing domains formed that were separated by a DW ("onion state"). The DW trapped the SPM beads, and was shifted along the conduit perimeter by an in-plane rotating magnetic field. The magnetic field drove the beads around the perimeter at a velocity up to 1000 µm/s. Reprinted with permission from E. Rapoport and G. S. D. Beach, Physical Review B, 2013, 87, Copyright 2013 by the American Physical Society.[110]

3.6 Multi-frequency external driven separation

View Article Online
DOI: 10.1039/C6LC00707D

A promising separation strategy based on multi-frequency driven bead transport was introduced by Tierno, *et al.* in stripe patterned and bubble DW substrates.[81, 84] SPM beads were transported across the film due to the effect of the in-plane component of an applied magnetic field that modified the strength of adjacent pinning sites, combined with the perpendicular component of the magnetic field that altered the size of the magnetic domains. A threshold existed for the magnitude of the in-plane component of the magnetic field, H_{xy}, below which the beads remained pinned to the initial location, and above which the transport was enabled. As in NLM this threshold field for a SPM bead depended on the distance between the DW and the bead centre, so that larger beads had a lower threshold and were more easily transported. This feature was exploited for bead separation by imposing a multi-frequency modulation to the applied field

$$[\boldsymbol{H_x}, \boldsymbol{H_z}] = [\boldsymbol{sin}(\boldsymbol{\omega_x}\, \boldsymbol{t}), \boldsymbol{sin}(\boldsymbol{\omega_z}\, \boldsymbol{t})], \quad (10)$$

where ω_x is an integer multiple of ω_z. In this configuration the in-plane field oscillated faster than the perpendicular field, so that H_z pointed in different directions when the in-plane component of the field overcame the threshold for different magnetic beads (1 µm and 2.8 µm). For example, if $\omega_x = 3\ \omega_z$, during a cycle the larger beads hopped twice in the forward direction and once in the backward direction, whereas the smaller beads hopped only once in the backward direction (Figure 11). The authors demonstrated efficient separation of the two bead populations, and used the technique to separate small bead - large bead complexes formed by the cross-linking of complementary DNA strands present on the beads' surface.

A similar separation principle was also demonstrated in a bubble domain lattice for 1 µm and 2.8 µm beads. By tuning the normal component of the applied field it was possible to impose different transport regimes to the beads, depending on their size. At low H_z the two bead types exhibited a circular orbit around a bubble domain. For increasing H_z the larger beads started travelling across the lattice while the smaller beads remaining in a closed orbit. At higher values of H_z both the bead populations were free to move. For further increases in H_z the larger beads entered a closed orbit regime while the smaller beads continued their free motion.

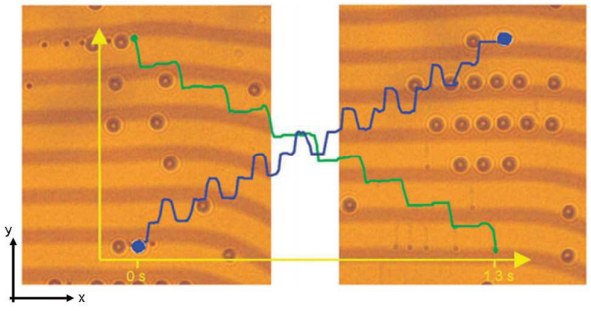

Fig. 11 Size based multi-frequency driven bead separation. The dark and light stripes in the thin magnetic film correspond to oppositely oriented magnetic domains. An in-plane rotating magnetic field and a perpendicular rotating magnetic field were applied. A threshold existed for the magnitude of the in-plane component of the magnetic field, below which the beads remained pinned to their initial location. The threshold depended on the bead properties, so that by imposing a difference in the rotational frequencies of the applied fields it was possible to achieve size selective bead separation: over a field cycle (with $\omega_x = 3\ \omega_z$), the larger beads hopped twice in the forward direction and once in the backward direction, whereas the smaller beads hopped only once in the backward direction. Reproduced from Ref. [84] with permission from The Royal Society of Chemistry.

The multi-frequency approach was also investigated in circular patterned micromagnets for the separation of 2.8 µm beads from 5.8 µm beads.[67, 70] The external magnetic field was applied rotating in the *xz*-plane with a frequency and a phase difference between the two components. The ratio between the driving frequencies, $R_f = \omega_z / \omega_x$, determined the transport regime of the SPM beads: (i) for odd integer ratios, *i.e.* 7/5 or 9/5, the beads went through a sequence of forward and backward steps, (ii) for even or irrational ratios the beads exhibited only closed orbit, *i.e.* zero averaged velocity. The phase difference ϕ_0 influenced the direction of motion and the type of trajectory, *i.e.* open or closed: narrow phase intervals were found in which the smaller beads exhibited closed orbits, while the larger beads travelled across the micromagnets, thus enabling on-chip separation. A thorough theoretical analysis of this transport behaviour was presented by Ouyang, *et al.* describing the effect of the static forcing terms generated by the micromagnet array.[70] This separation approach has a significant difference over the critical-frequency based separation described in the previous sections: simultaneous transport of the beads in opposite directions reduces the undesired immobilisation of travelling beads blocked by immobile beads. This made it possible to transport smaller beads at the expense of larger beads, a regime that was not present in the previous configuration.

In summary, we have reviewed the transport and separation capabilities of micromagnetic arrays and thin films. These devices allow the transportation of individual beads with submicron resolution, without the need for hydrodynamic flow. These devices have allowed individual beads to be transported, analysed, and isolated based on their size, magnetic moment, and the presence of non-magnetic materials bound to the beads. The fact that hydrodynamic flow is not required eliminates the need for carrier fluids and fine control of hydrodynamic forces. The main limitation of the micromagnet arrays lies in the lower bead throughput, *i.e.*, hydrodynamic flow increases the rate of transport and separation of beads up to tens of thousands beads per second. This limitation can in principle be overcome by using multiple elements working in parallel, thus simultaneously transporting and separating numerous beads.

4 Multi-element micromagnet design for bioanalytical systems

Magnetically driven microsystems need a number of common functional operations, *i.e.*, collection, switching, reaction, separation, and detection. This section describes micromagnet structures that have been designed to expand the performance beyond the arrays that have been introduced so far. Early work on SFE arrays focused on separating specific SPM beads using the orientation of the in-plane magnetic field H_{xy}. Figure 12a presents a micromagnetic trap developed by Gunnarsson et al. with a pattern of orthogonally arranged ellipses.[40, 42] Beads were trapped in loops

View Article Online
DOI: 10.1039/C6LC00707D

by controlling the sense of rotation of the applied field, *i.e.*, the SPM beads travelled along the perimeter of the ellipses clockwise (Figure 12a-i) or counter clockwise (Figure 12a-ii). This feature was used to separate SPM beads by sequentially switching the sense of rotation of the applied magnetic field, *i.e.*, the SPM beads entered a loop structure for clockwise rotation while they continued traveling along the micromagnets for counter clockwise rotation. Figure 12b presents trapping stations formed by 5 µm half-disk micromagnets studied by Venu, *et al.*.[53] The evolution of the local magnetic field on a pattern of connected half-disks made the SPM beads travel a distance *2d* for each field cycle, where *d* is the characteristic dimension of the array (24 µm/s at 1 Hz). The micromagnet loops were used to trap 2.8 µm SPM beads and magnetically labelled *Cyanobacterium Synechocystis*. In this configuration the trapped SPM beads could not escape from the trapping stations, due to a local potential energy barrier created at the T-junction (bottom left-hand side of the loop), *i.e.*, once the SPM beads entered the loop they travelled along its internal perimeter following the sense of rotation of the applied field. Therefore, the inversion of the sense of rotation also trapped the bead-organism complex inside the loop while preventing other SPM beads from entering the trapping station.

An advance in switching-separation micromagnet design was recently demonstrated with the integration of on-chip current-carrying wires (Figure 12c), which increased the complexity of the device, but enabled local operational control.[56, 57] The electromagnetic field allowed the local magnetic field at the T-junction to be modulated, suppressing the energy barrier that prevented the beads from escaping the loop structure. With this strategy it was possible to selectively separate SPM beads by synchronising the applied current with the rotating magnetic field. This functionality was integrated in a complex network of micromagnets and current-carrying wires to create an array of programmable trapping sites. The on-chip current wires also enabled a novel separation approach, based on a gap inserted in a line of circular micromagnets connected by a thin magnetic strip (Figure 12d).[56] The SPM beads travelled in the positive *x*-direction along the top part of the micromagnet line; when the beads reached the gap they rotated around the perimeter of the last micromagnet following the rotation of the applied magnetic field H_{xy}, and continued their motion in the negative *x*-direction travelling along the bottom part of the line. A current-carrying wire was used to create a switch-separator in which local electromagnetic field attracted the beads to the other side of a gap (Figure 12d). The synchronisation of the current (around 3 mA) with the applied magnetic field enabled the precise separation of travelling beads. The switching efficiency increased with the size of the SPM beads relative to the disk diameter.[57] However, larger beads also had a tendency to cross the gap even without the applied gate current, thus causing a "leakage" of beads. This leakage could be prevented by applying a negative bias current. The optimum bead diameter for maximising the switching efficiency was estimated to be approximately one half the magnet diameter.[57]

Figure 12e presents a bifurcated DW-nanowire designed by Torti, *et al*. for SPM bead separation.[106] A zig-zag nanowire interfaced with a demultiplexer unit formed by two opposite branches was tilted by +5° or -5° with respect to the horizontal axis of the chip. The SPM beads that reached the end of this path were transported to the sorting unit. Then, the rotation of the external field was tilted by a positive (negative) angle with respect to the *x*-direction, and transported the beads along the upper (lower) branch of the circuit. The authors demonstrated the capabilities of the system by showing the sequential separation of 1 µm and 2.8 µm beads. However, a precise tuning of the applied field synchronously with the position of the SPM beads was required to drive the beads along the desired path.

View Article Online
DOI: 10.1039/C6LC00707D

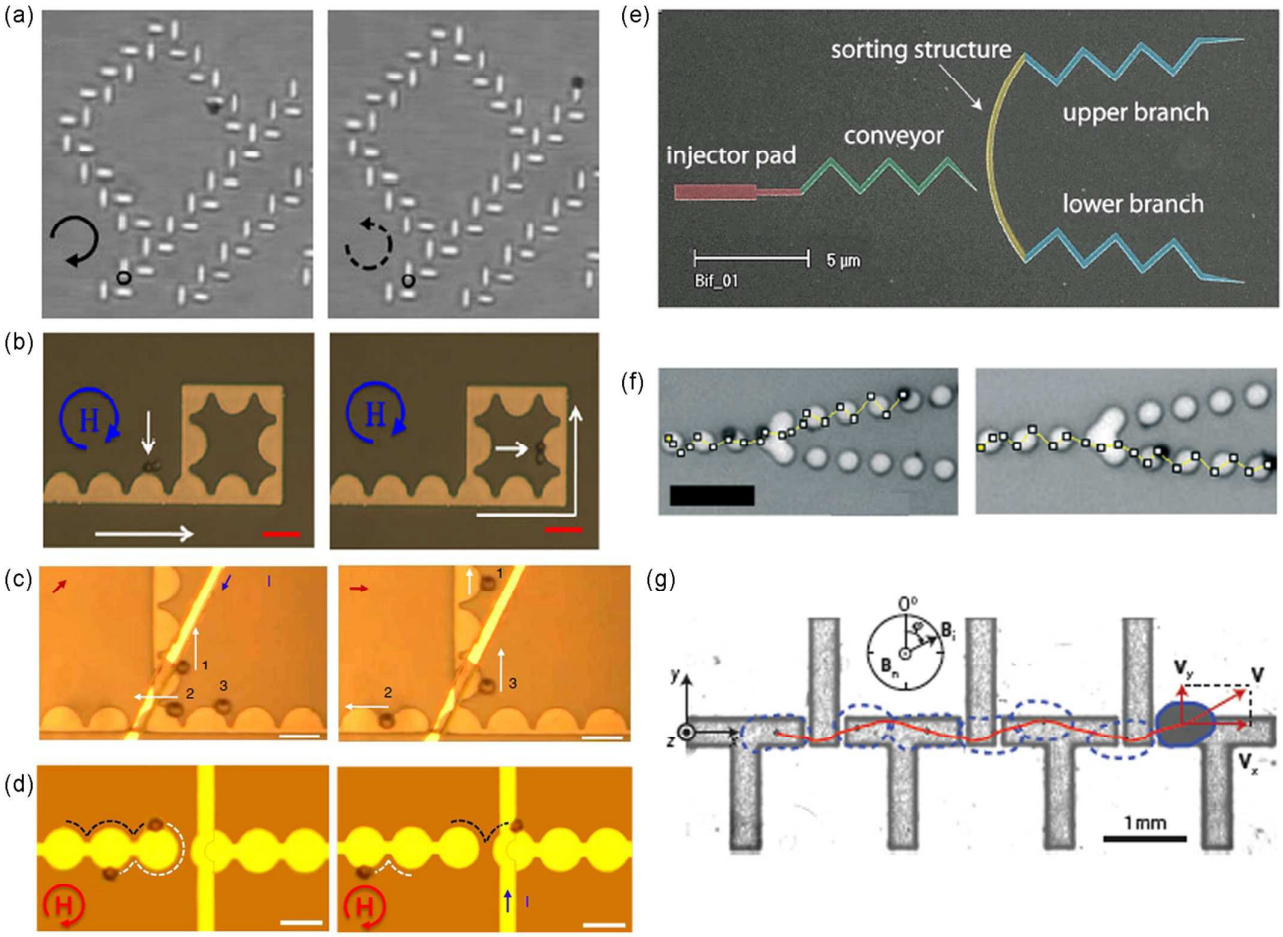

Fig. 12 Multi-element micro-magnetic structures (a) Loop trapping stations formed by orthogonal lines of elliptical micromagnets. The beads traveled along the perimeter of the ellipses following the rotation of the in-plane magnetic field, and jumped from one element to the adjacent one. Depending on the sense of rotation of the in-plane field, the SPM beads entered the loop or escaped from it.[39] Reproduced with permission (b) Loop trapping stations formed by half-disk micromagnets. The beads traveled along the perimeter of the elements following the rotation of an in-plane magnetic field. A potential energy barrier was created by the T-junction on the bottom left-hand side of the loop, which prevented the beads from escaping it.[52] Reproduced with permission of Springer (c) The addition of a current-carrying line allowed modulating the local potential energy landscape, and suppressing the potential energy barrier, thus enabling the release of SPM beads from the loop structures.[55] (d) Separation strategy based on a gap inserted in a line of circular micromagnets. The SPM beads travelled along the top part of the line following the rotation of an in-plane magnetic field. When the beads reached the gap they inverted their motion and travelled along the bottom part of the line. If a current was applied, it created a local magnetic field maximum on the opposite side of the gap that attracted the beads.[55] (e) DW conduit sorting structure. The SPM beads were transported along the conveyor part of the circuit by the shifting of the DWs induced by an applied in-plane rotating magnetic field. When the beads reached the end of the conveyor part, they jumped to the upper (lower) branch if the applied field was tilted by a positive (negative) angle with respect to the horizontal axis of the chip. Reprinted from A. Torti, V. Mondiali, A. Cattoni, M. Donolato, E. Albisetti, A. M. Haghiri-Gosnet, P. Vavassori and R. Bertacco, Appl Phys Lett, 2012, 101, 142405, with the permission of AIP Publishing.[104] (f) Trimagnet switching junction formed by permanent micromagnets. The beads were transported by an out-of-plane rotating field. The magnetisation of the micromagnets was tilted by a negative (positive) angle, thus transporting the SPM beads along the upper (lower) branch due to the local potential energy landscape evolution. Bead separation was enabled by the inversion of the bead behaviour above a threshold magnetisation angle that was dependent on the bead properties. Reproduced from Ref. [70] with permission from The Royal Society of Chemistry. (g) T- and I-shaped magnetic structures used to form transport lines for ferromagnetic droplets. The droplets were driven by the rotation of an in-plane magnetic field. The patterned features were used to create logic gates and enable Boolean operations on-chip. Reprinted by permission from Macmillan Publishers Ltd: G. Katsikis, J. S. Cybulski and M. Prakash, Nature Physics, 2015, copyright 2015.[57]

A size-selective sorting structure has recently been implemented with a HME tri-magnet junction in which a single line of magnets split into two branches (Figure 12f).[72] This separator was based on the relative orientation of the micromagnet magnetisation with respect to the applied rotating field (H_{xz}). When the micromagnets were magnetised along the *x*-direction (in-line with the micromagnet array), the beads randomly selected one of the two possible paths. If the magnetisation was tilted by a negative

View Article Online
DOI: 10.1039/C6LC00707D

(positive) angle α, beads were guided towards the upper (lower) branch of the junction by the evolution of the local magnetic field landscape, thus enabling a magnetic switching functionality. For high values of positive (negative) α the beads inverted their behaviour and jumped to the upper (lower) path after crossing the junction. This allowed continuous bead separation, as the threshold α value was dependent on the beads' size, *i.e.*, larger beads switched at lower α angles than smaller beads. The separation of 2.8 µm beads from 5.5 µm beads was demonstrated at the tri-magnet junctions. The properties of the junctions, such as size of the micromagnets and spacing between the two branches, may be adjusted to enhance the separation capabilities of the system.

A novel switch was recently proposed by Katsikis, *et al.*.[58] A pattern of 'T'-shaped and 'I'-shaped magnetic structures (Figure 12g) were assembled with an external in-plane rotating magnetic field that was used to control the transport of ferrofluid droplets. Similarly to the SPM beads, the transport dynamics of the ferrofluid droplets was influenced by the rotational frequency of the applied field: below a threshold frequency the droplets travelled synchronously with the rotating field, whereas above a threshold frequency they exhibited an asynchronous behaviour. The authors suggested that the droplets could be used as 'bits' to store and propagate information across the chip, *i.e.*, the absence or the presence of a

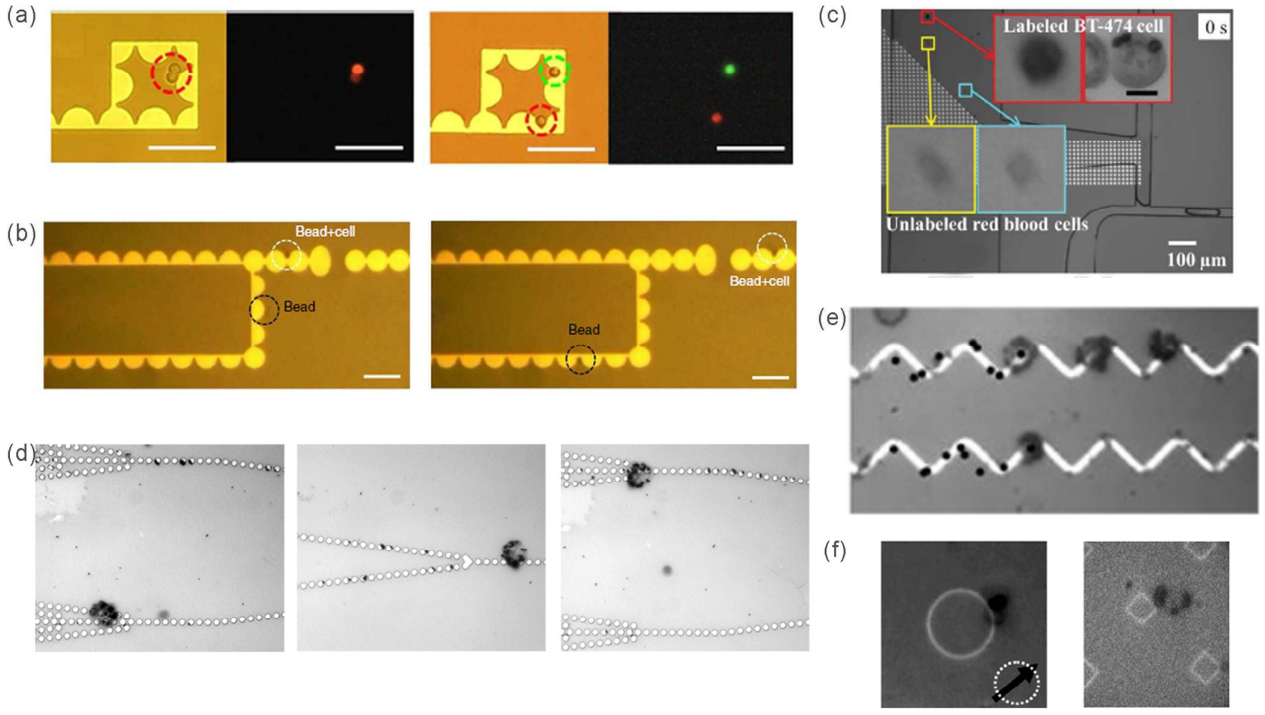

Fig. 13 On-chip cell manipulation with magnetic microstructures (a) Loop trapping stations for the precise positioning of single cells or cell pairs labelled with SPM beads. The bead-cell pairs were transported by an in-plane rotating magnetic field, and were trapped in the loop structures by a potential energy barrier. The biological activity of the cells was monitored on-chip, such as cell mitosis.[55] Reproduced with permission (b) Critical frequency-based separation of bead-cell complexes from unreacted beads on a gap structure. The bead transport was governed by an in-plane rotating magnetic field. The bead-cell complexes had lower critical frequency than the bare beads, so that they were in the "phase-slipping" regime and were shuttled across the gap, whereas the bare beads inverted their motion.[55] Reproduced with permission (c) Encapsulation of cells in droplets. Cells labelled with SPM beads were separated from un-labelled cells in a circular micromagnet array. The bead-cell complexes were then driven by an external rotating magnetic field towards a region in which an applied hydrodynamic flow created droplets in which the cells were encapsulated, and were transported in a secondary flow stream. Reproduced from Ref. [53] with permission from The Royal Society of Chemistry. (d) Programmed transport of a breast cancer cell labelled with 1 µm SPM beads. The cell was initially magnetically focused and transported across a trimagnet junction by an out-of-plane rotating field. The field direction was then inverted, thus transporting the cell backwards across the junction. By tilting the micromagnet magnetisation by a positive (negative) angle, it was possible to induce a preferential direction for the cell at the junction, *i.e.* lower (upper) branch. Reproduced from Ref. [70] with permission from The Royal Society of Chemistry. (e) Labelled cell transport along a DW zigzag conduit due to an in-plane rotating field that shifted the position of the DWs along the conduit. The black dots indicate the time-evolution of the cell position. Reprinted with permission from G. Vieira, T. Henighan, A. Chen, A. Hauser, F. Yang, J. Chalmers and R. Sooryakumar, Physical review letters, 2009, 103, 128101, Copyright 2009 by the American Physical Society.[92] (f) Labelled cell trapping and transport in square and circular DW conduits. The position of the cells was controlled with sub-µm precision by applying an in-plane rotating field. Reproduced from Ref. [101] with permission from The Royal Society of Chemistry.

View Article Online
DOI: 10.1039/C6LC00707D

droplet in a specific location would correspond to a value 0 or 1, respectively. On-chip Boolean logic operations were implemented by suitably patterning a sequence of 'T'- and 'I'-shaped structures to create AND/OR and XOR/AND gates. These gates were then used as building blocks to create a NAND gate and a full adder. The on-chip magnetic structures were also capable of extracting new ferrofluid droplets from a reservoir, thus providing constant input to the chip. The authors envisioned the application of this strategy for creating fully functional logic circuits that would allow the simultaneous manipulation of thousands of nanolitre droplets, thus enabling fast and parallel transfer of information.

In this section, micromagnet designs for collection, switching, reaction, separation, and detection of SPM beads have been reviewed. Loop traps appear to constitute a powerful platform for the isolation of specific SPM beads, diverging junctions enable continuous bead separation, and the magnetic logic gates can create fully functional logic circuits. Future development of these technologies needs to focus on increasing the rate of processing beads. This can be achieved through the implementation of networks of trapping stations and diverging junctions that can simultaneous transport and separate tens of thousands of beads per second.

5 Controlled cellular manipulation

One of the most important bioanalytical applications of SPM beads is the specific labelling of cell populations for the separation of specific cell types from heterogeneous mixtures that result from biomedical and biotechnology applications.[121] Magnetic microstructures provide a means for separating and trapping cells in precise locations of the chip, thus facilitating analysis at the single cell level. In this section we summarise the most relevant findings that highlight the potential of magnetic microstructures for cellular manipulation.

The first example of cell manipulation was performed with nonlinear magnetophoretic separation.[64] Yeast cells labelled with SPM beads were transported across an array of circular micromagnets, and were separated from unreacted beads due to the lower critical frequency. Cell manipulation in a more complex micromagnet network was demonstrated by Lim, *et al.*.[56] B- and T-lymphocytes labelled with SPM beads were transported across half-disk micromagnets and trapped in magnetic loop structures (Figure 13a). The trapping station allowed compartmentalising single cells or cell pairs, thus providing a means for preparing samples for analysis at the single-cell level. Cell activity was monitored on-chip, thus allowing real time analysis of biological processes such as mitosis. The lower critical frequency of the bead-cell complexes was exploited for separation on a gap structure (Figure 13b), *i.e.*, the "phase-slipping" transport regime of the bead-cell complexes allowed them to be shuttled across the gap, while the bare beads inverted their direction of motion.
Chen, *et al.*, combined the magnetic manipulation capabilities of microfabricated magnets with precise flow control to encapsulate magnetically labelled BT-474 cells in microlitre droplets (Figure 13c).[54] The cell compartmentalisation in droplets facilitated the preservation of the cell activity, and the droplets could be used as microreactors for testing different treatments. The labelled cells were captured by the patterned micromagnets from a heterogeneous population of red blood cells, and were magnetically driven in a secondary flow stream for the encapsulation in droplets. The authors demonstrated an on-chip sorting mechanism and demonstrated the preserved cell viability via fluorescent measurements.

Magnetic "switch junctions" have been employed for isolation and programmable manipulation of labelled breast cancer cells from dilute serum samples. These model circulating tumour cells were initially collected on a large rectilinear array of circular micromagnets and then "focused" through converging micromagnet lines (Figure 13d). Optical monitoring allowed the sense of rotation of the applied field to be inverted and the cells were transported backwards through a tri-magnet split junction where they took a preferential direction imposed by the magnetisation of the micromagnets. Thus, the author demonstrated guided cell transport across the magnet array .[72]

Cell manipulation and transport has also been demonstrated for DW zigzag wires.[96, 104] The wire geometry allowed trapping the cells at specific locations, releasing them by applying a suitable hydrodynamic flow, and transporting them along the zig-zag pattern (Figure 13e). The activity of the cells was not affected by the magnetic labelling or manipulation, enabling the study of single cellular behaviour over long periods of time. In addition to the wire geometry, square and circular DW conduits (Figure 13f) also enabled cell trapping.[104]

Magnetic labelling is not a strict requirement for on-chip cell manipulation with microfabricated magnetic features. The SPM beads may act as miniaturised force-transmitting probes to guide the motion and the assembly of un-labelled cells. Henighan, *et al.*, demonstrated this approach in patterned circular de-magnetisable elements.[48] *Leukemia* cells were arranged in ordered structures by the multi-directional motion of SPM beads, and were transported across the surface at a velocity up to 20 µm/s. The transport of un-labelled cells was demonstrated also on FGFs by Tierno et al..[79, 84] The motion of the SPM beads across the thin magnetic film caused a secondary flow that allowed the transport of yeast cells suspended 1-2 µm above the surface. The cells were transported in the same direction of the travelling beads, at approximately half the speed (up to 100 µm/s).

Thus, magnetic microstructures enable a high degree of control over magnetically labelled and un-labelled cells in LOC devices. The position of the cells can be controlled with sub-µm precision, and engineered structures may be used to achieve on-chip trapping. Specific cell populations can be isolated from complex samples, and the cells of interest can be compartmentalised alone or in pairs for monitoring their activity. Analysis at the singe cell level is enabled by the separation capabilities of the magnetic microstructures, thus facilitating the investigation of complex cellular behaviours.

View Article Online
DOI: 10.1039/C6LC00707D

It is informative to compare the capabilities of micromagnet systems with miniaturised linear magnetophoretic devices that use hydrodynamic flow to isolate magnetically labelled cells and bacteria.[122-126] Linear magnetophoresis has been demonstrated on LOC devices for the isolation of specific cell populations from complex fluids, and multiplexing has been achieved using magnetic beads functionalised with antibodies targeting different cell types. These linear devices have achieved reasonably high throughput, *i.e.*, isolation of 1000s or 10,000s cells/s, with purity and enrichment greater than 90%. However, further analysis of the cell populations is required after the separation in order to characterize the isolated cells and determine separation efficiency. Moreover, a precise balancing of hydrodynamic and magnetic forces is required to operate such a device. Systems based on micromagnets can be used to collect magnetically labelled cells at a density of 100,000 cells/cm^2. The analysis of these cells can be rapidly implemented by using NLM to first remove the unwanted bare SPM beads and then identify specific types of cells labelled with SPMs based on their size or magnetisation. Micromagnet systems also allow single cells labelled with magnetic beads to be isolated for further analysis, although the throughput of these systems will be much lower.

Another interesting comparison is with devices based on microfabricated electromagnets that have been used to manipulate and separate cells and bacteria at the microscale.[31, 127, 128] For example, matrices of current-carrying wires enabled the separation of viable from non-viable cells, and the controlled assembly of cell populations in specific areas of the chip. The advantage of this technique is that single wires can be addressed to manipulate single cells. However, as mentioned in the Introduction, microelectromagnets present challenges in terms of complexity of fabrication and operation, *i.e.*, each wire needs a regulated, dedicated current source.

6 Other applications

On-chip magnetic elements have been used to tune the assembly of magnetic beads to create asymmetric 'janus' particles. The shape and the density of these bead assemblies was controlled by the applied rotating field,[55] which also enabled the transport of the bead aggregates. Yellen, *et al*. demonstrated the manipulation and the controlled assembly of nonmagnetic particles immersed in a ferrofluid using arrays of circular HME micromagnets.[62, 63] When an external field was applied, the magnetic and nonmagnetic particles positioned themselves in the regions of maximum and minimum magnetic field, respectively. A variety of ordered particle structures were observed, which were dependent on the relative size of the particles with respect to the size of the micromagnets, and on the concentration of magnetic nanoparticles in the ferrofluid. Hexagonal and cubic structures were created by properly tuning the experimental parameters. The controlled assembly and transport of SPM beads was also demonstrated on thin magnetic films and DW conduits.[87, 88, 99] DW-bead interactions were regulated by coating the magnetic films with a nonmagnetic layer,[87] and the bead transport was used to induce motion in nonmagnetic particles suspended above the substrate. Prikockis, *et al.* studied the assembly of SPM beads at the vertices of zig-zag magnetic wires.[99] Under the influence of a perpendicular magnetic field, the SPM beads aggregated over time maintaining a well-defined order. The external field H_z offered a mean to control the symmetry and the stability of the bead clusters, which were also transported along the zig-zag wires, thus providing full control over the magnetic beads.

The rotation of SPM beads around microfabricated magnetic elements patterned inside microfluidic channels has been controlled to perturb their hydrodynamic conditions, thus providing localised control of flow regimes in LOC devices. Henigan, *et al.* demonstrated this approach with 10 µm microfabricated de-magnetisable disks and cavities (circular holes in a magnetic film) inside a microfluidic chamber.[49] These magnetic structures trapped the SPM beads that rotated around the perimeter of the elements following an applied in-plane magnetic field. The rotation of the beads increased the velocity of the surrounding fluid (up to 10 µm/s). Tuning the sense of rotation of the applied field controlled the direction of the flow. An important parameter was the width of the gap between the magnetic elements and the walls of the microfluidic channels.[52] The highest pumping efficiency was achieved by minimising the gap width, *i.e.*, increased asymmetry in the flow profile enhanced the pumping process. A similar strategy was used by Peng, *et al.* to induce mixing in a microfluidic channel.[50] The rotation of SPM beads around the perimeter of circular de-magnetisable elements (up to 1000 µm/s) was used for the active mixing of two flowing solutions. Similarly, the motion of SPM bead chains across a DW substrate was proven to induce mixing between fluids in a microfluidic chamber.[92]

Recently, micromagnets have been used for the controlled application of localised forces and mechanical stress on thousands of immobilised cells simultaneously.[129] This application involves a time-varying magnetic field for studying the mechanical response of cancer cells to applied forces, a feature which is of particular importance for understanding complex mechanotransduction processes. Applied field, however, is not exploited for the transport of cells, which are lithographically patterned on the surface. This particular application could be integrated in LOC devices based on micromagnetic features and rotating magnetic fields to create a bioanalytical systems capable of transporting, separating and exerting controlled forces on cells of interest.

In this section we reviewed emerging applications of micromagnets. The efficiency of pumps and mixing devices is not very high, but these operations can be exploited in microsystems designed for bead and cell transport and separation. Arrays of micromagnetic also appear to be a promising tool for rapidly assembling magnetic structures and characterising the mechanochemical properties of cells.

7 Conclusions and outlook

In this article we have reviewed micromagnet technology as it applies to bioanalytical systems. The highly localised magnetic field (and field gradient) generated by miniaturised magnetic features enable micrometre scale control of individual SPM beads and magnetically labelled bioanalytes. The magnetic fields required to move the SPM beads are generated by external electromagnets and allow *ca.* 10^5 SPM beads to be simultaneously manipulated over

View Article Online
DOI: 10.1039/C6LC00707D

cm^2 areas with relatively low levels of power consumption. This technology has been successfully applied to a range of bioanalytical operations, such as, transport, switching, mixing, separation, and detection of magnetically labelled biological analytes.

Magnetically driven systems based on micromagnet structures meet the requirements of fully functional *in vitro* diagnostic and point of care testing. Advantages of the micromagnet systems are that they enable rapid and high efficiency magnetic isolation of bioanalytes from millilitre volumes of complex samples based on the size and magnetisation of the SPM bead-bioanalyte complex. These systems are well suited for multiplexed biosensing applications based on magnetic and optical detectors. Additional advantages of micromagnet arrays in biosensing are that they minimise liquid consumption and the need for precise control of the hydrodynamics. The ease of detection of analytes at the single bead level with this technology will enable *in vitro* analysis to be performed a very high level of sensitivity and specificity. SPM bead-based isolation of rare cells and other bioanalytes from blood samples using micromagnets promises to facilitate the early detection of biomarkers and monitoring of therapeutics for diseases such as cancer.

What is missing in the field and where should it go next? The throughput of LOC devices based on micromagnetic elements has been limited and is lower than systems that operate with hydrodynamic flow. Thus, the demonstration of micromagnetic systems that operate with > 10^7 SPMs is needed for bringing this powerful technology closer to the market. Another feature that would help in this regard and enhance the capabilities of micromagnetic devices is an integrated detection system for the real time analysis of SPM beads and associate biological analytes. The fact that the beads and the biological targets travel synchronously and individually rather than in aggregates should be exploited for automated counting and for studying their properties such as size, optical properties and aggregation state during their motion. This detection system would eliminate the need for post-processing characterisation, thus reducing the total time of the analysis and loss of bioanalyte due to nonspecific adsorption.

Acknowledgements

This work was supported by the Science Foundation of Ireland (IJ08/RP1/B1376; 08/IN1/B2072), Irish Research Council, and the Nanoremedies Programme funded under the Programme for Research in Third-Level Institutions of Ireland and co-funded under the European Regional Development fund.

Notes and references

1. J. Kaiser, *Science*, 2010, **327**, 1072-1074.
2. Q. A. Pankhurst, J. Connolly, S. K. Jones and J. Dobson, *Journal of Physics D: Applied Physics*, 2003, **36**, R167-R181.
3. M. A. M. Gijs, *Microfluidics and Nanofluidics*, 2004, DOI: 10.1007/s10404-004-0010-y.
4. T. Neuberger, B. Schöpf, H. Hofmann, M. Hofmann and B. Von Rechenberg, *Journal of Magnetism and Magnetic Materials*, 2005, **293**, 483-496.
5. C. Fields, P. Li, J. J. O'Mahony and G. U. Lee, *Biotechnology and Bioengineering*, 2015, DOI: 10.1002/bit.25665, n/a-n/a.
6. N. Pamme, *Curr Opin Chem Biol*, 2012, **16**, 436-443.
7. M. Zborowski and J. J. Chalmers, *Analytical chemistry*, 2011, **83**, 8050-8056.
8. W. Rieman and H. F. Walton, *Ion Exchange in Analytical Chemistry: International Series of Monographs in Analytical Chemistry*, Elsevier, 2013.
9. P. Xu, D. M. Duong and J. Peng, *Journal of proteome research*, 2009, **8**, 3944-3950.
10. L. Tucker, *BCC Research*, 2013.
11. N. Pamme, *Lab Chip*, 2006, **6**, 24-38.
12. M. Karle, J. Miwa, G. Czilwik, V. Auwarter, G. Roth, R. Zengerle and F. von Stetten, *Lab Chip*, 2010, **10**, 3284-3290.
13. N. Pamme and A. Manz, *Anal Chem*, 2004, **76**, 7250-7256.
14. D. Robert, N. Pamme, H. Conjeaud, F. Gazeau, A. Iles and C. Wilhelm, *Lab Chip*, 2011, **11**, 1902-1910.
15. T. P. Forbes and S. P. Forry, *Lab Chip*, 2012, **12**, 1471-1479.
16. K. Hoshino, Y. Y. Huang, N. Lane, M. Huebschman, J. W. Uhr, E. P. Frenkel and X. Zhang, *Lab Chip*, 2011, **11**, 3449-3457.
17. P. Chen, Y.-Y. Huang, K. Hoshino and J. X. Zhang, *Scientific reports*, 2015, **5**.
18. A. Rida and M. A. M. Gijs, *Applied Physics Letters*, 2004, **85**, 4986.
19. S. H. Lee, D. van Noort, J. Y. Lee, B. T. Zhang and T. H. Park, *Lab Chip*, 2009, **9**, 479-482.
20. Y. Gao, A. van Reenen, M. Hulsen, A. De Jong, M. Prins and J. den Toonder, *Microfluidics and nanofluidics*, 2014, **16**, 265-274.
21. A. Ranzoni, J. J. Schleipen, L. J. van Ijzendoorn and M. W. Prins, *Nano Lett*, 2011, **11**, 2017-2022.
22. B. McNaughton, R. Agayan, J. Wang and R. Kopelman, *Sensors and Actuators B: Chemical*, 2007, **121**, 330-340.
23. A. Hecht, P. Kinnunen, B. McNaughton and R. Kopelman, *J Magn Magn Mater*, 2011, **323**, 272-278.
24. Y. Moser, T. Lehnert and M. A. Gijs, *Lab Chip*, 2009, **9**, 3261-3267.
25. W.-S. Chang, H. Shang, R. M. Perera, S.-m. Lok, D. Sedlak, R. J. Kuhn and G. U. Lee, *Analyst*, 2008, **133**, 233-240.
26. T. Deng, M. Prentiss and G. M. Whitesides, *Applied physics letters*, 2002, **80**, 461-463.
27. M. Berger, J. Castelino, R. Huang, M. Shah and R. H. Austin, *Electrophoresis*, 2001, **22**, 3883.
28. C. H. Ahn, Y. J. Kim and M. G. Allen, *Components, Packaging, and Manufacturing Technology, Part A, IEEE Transactions on*, 1994, **17**, 463-469.
29. C. H. Ahn, M. G. Allen, W. Trimmer, Y.-N. Jun and S. Erramilli, *Microelectromechanical Systems, Journal of*, 1996, **5**, 151-158.
30. C. S. Lee, H. Lee and R. M. Westervelt, *Applied Physics Letters*, 2001, **79**, 3308.
31. H. Lee, A. M. Purdon and R. M. Westervelt, *Applied Physics Letters*, 2004, **85**, 1063.

View Article Online
DOI: 10.1039/C6LC00707D

32. K. Smistrup, O. Hansen, H. Bruus and M. F. Hansen, *Journal of Magnetism and Magnetic Materials*, 2005, **293**, 597-604.
33. Y. Zheng, A. Mannai and M. Sawan, *Microelectronic Engineering*, 2014, **128**, 1-6.
34. Q. Ramadan, C. Yu, V. Samper and D. P. Poenar, *Applied physics letters*, 2006, **88**, 032501.
35. Q. Ramadan and L. T. Ting, *Microelectromechanical Systems, Journal of*, 2011, **20**, 1310-1323.
36. A. Rida, V. Fernandez and M. A. M. Gijs, *Applied Physics Letters*, 2003, **83**, 2396.
37. J. G. Kim, K. H. Han, S. H. Song and A. Reilly, *Thin Solid Films*, 2003, **440**, 54-59.
38. N. V. Myung, D. Y. Park, B. Y. Yoo and P. T. A. Sumodjo, *Journal of Magnetism and Magnetic Materials*, 2003, **265**, 189-198.
39. M. R. J. Gibbs, E. W. Hill and P. J. Wright, *Journal of Physics D-Applied Physics*, 2004, **37**, R237-R244.
40. K. Gunnarsson, P. E. Roy, S. Felton, J. Pihl, P. Svedlindh, S. Berner, H. Lidbaum and S. Oscarsson, *Advanced Materials*, 2005, **17**, 1730-1734.
41. S. Felton, P. Warnicke, K. Gunnarsson, P. E. Roy, H. Lidbaum and P. Svedlindh, *Journal of Physics D: Applied Physics*, 2006, **39**, 610.
42. P. Warnicke, S. Felton, K. Gunnarsson and P. Svedlindh, *Journal of Magnetism and Magnetic Materials*, 2006, **303**, e294-e298.
43. R. S. Conroy, G. Zabow, J. Moreland and A. P. Koretsky, *Applied Physics Letters*, 2008, **93**, 203901.
44. S. Anandakumar, V. Sudha Rani, J. R. Jeong, C. Kim, K. W. Kim and B. P. Rao, *Journal of Applied Physics*, 2009, **105**, 07B312.
45. L. Johansson, K. Gunnarsson, S. Bijelovic, K. Eriksson, A. Surpi, E. Gothelid, P. Svedlindh and S. Oscarsson, *Lab Chip*, 2010, **10**, 654-661.
46. S. Anandakumar, V. S. Rani, S. Oh, B. L. Sinha, M. Takahashi and C. Kim, *Biosens Bioelectron*, 2010, **26**, 1755-1758.
47. G. Ruan, G. Vieira, T. Henighan, A. Chen, D. Thakur, R. Sooryakumar and J. O. Winter, *Nano Lett*, 2010, **10**, 2220-2224.
48. T. Henighan, A. Chen, G. Vieira, A. J. Hauser, F. Y. Yang, J. J. Chalmers and R. Sooryakumar, *Biophys J*, 2010, **98**, 412-417.
49. T. Henighan, D. Giglio, A. Chen, G. Vieira and R. Sooryakumar, *Applied Physics Letters*, 2011, **98**, 103505.
50. Z. C. Peng, P. Hesketh, W. Mao, A. Alexeev and W. Lam, 2011.
51. B.-H. Lim, I.-G. Jeong, S. Anandakumar, K. W. Kim and C.-G. Kim, *Journal of Magnetics*, 2011, **16**, 363-367.
52. W. T. E. v. d. Beld, I. E. L. d. Weerd, D. i. L. Abelmann, I. J. G. Bomer, P. d. i. A. v. d. Berg and D. J. C. T. Eijkel, presented in part at the MicroTAS 2012, 16th International Conference on Miniaturized Systems for Chemistry and Life Sciences, Okinawa, Japan, 2012.
53. R. Venu, B. Lim, X. H. Hu, I. Jeong, T. S. Ramulu and C. G. Kim, *Microfluidics and Nanofluidics*, 2012, **14**, 277-285.
54. A. Chen, T. Byvank, W. J. Chang, A. Bharde, G. Vieira, B. L. Miller, J. J. Chalmers, R. Bashir and R. Sooryakumar, *Lab Chip*, 2013, **13**, 1172-1181.
55. A. Chen and R. Sooryakumar, *Scientific reports*, 2013, **3**.
56. B. Lim, V. Reddy, X. Hu, K. Kim, M. Jadhav, R. Abedini-Nassab, Y.-W. Noh, Y. T. Lim, B. B. Yellen and C. Kim, *Nat Commun*, 2014, **5**.
57. R. Abedini-Nassab, D. M. Murdoch, C. Kim and B. B. Yellen, *Journal of Applied Physics*, 2014, **115**, 244509.
58. G. Katsikis, J. S. Cybulski and M. Prakash, *Nature Physics*, 2015.
59. A. Chen, T. Byvank, G. B. Vieira and R. Sooryakumar, *Magnetics, IEEE Transactions on*, 2013, **49**, 300-308.
60. S. S. Shevkoplyas, A. C. Siegel, R. M. Westervelt, M. G. Prentiss and G. M. Whitesides, *Lab on a Chip*, 2007, **7**, 1294-1302.
61. K. van Ommering, J. H. Nieuwenhuis, L. J. van IJzendoorn, B. Koopmans and M. W. Prins, *Applied physics letters*, 2006, **89**, 142511-142511.
62. B. B. Yellen, O. Hovorka and G. Friedman, *Proc Natl Acad Sci U S A*, 2005, **102**, 8860-8864.
63. B. B. Yellen, R. M. Erb, D. S. Halverson, O. Hovorka and G. Friedman, *Magnetics, IEEE Transactions on*, 2006, **42**, 3548-3553.
64. B. B. Yellen, R. M. Erb, H. S. Son, R. Hewlin, Jr., H. Shang and G. U. Lee, *Lab Chip*, 2007, **7**, 1681-1688.
65. B. Yellen and L. Virgin, *Physical Review E*, 2009, **80**.
66. L. Gao, N. J. Gottron, 3rd, L. N. Virgin and B. B. Yellen, *Lab Chip*, 2010, **10**, 2108-2114.
67. L. Gao, M. A. Tahir, L. N. Virgin and B. B. Yellen, *Lab Chip*, 2011, **11**, 4214-4220.
68. M. A. Tahir, L. Gao, L. N. Virgin and B. B. Yellen, *Phys Rev E*, 2011, **84**.
69. P. Li, A. Mahmood and G. U. Lee, *Langmuir*, 2011, **27**, 6496-6503.
70. Y. Ouyang, M. A. Tahir, D. J. Lichtenwalner and B. B. Yellen, *Physical Review E*, 2012, **85**, 041407.
71. P. Li, D. Kilinc, Y.-F. Ran and G. U. Lee, *Lab on a Chip*, 2013, **13**, 4400-4408.
72. S. Rampini, D. Kilinc, P. Li, C. Monteil, D. Gandhi and G. U. Lee, *Lab on a Chip*, 2015, DOI: 10.1039/C5LC00581G.
73. P. Bruno, G. Bayreuther, P. Beauvillain, C. Chappert, G. Lugert, D. Renard, J. P. Renard and J. Seiden, *Journal of Magnetism and Magnetic Materials*, 1991, **93**, 605-608.
74. V. Alexandrakis, D. Kechrakos, N. Moutis, D. Niarchos, G. Hadjipanayis and I. Panagiotopoulos, *Journal of Applied Physics*, 2016, **119**, 5.
75. J. Happel and H. Brenner, *Low Reynolds number hydrodynamics: with special applications to particulate media*, Springer Science & Business Media, 2012.
76. L. Helseth, T. Fischer and T. Johansen, *Physical Review E*, 2003, **67**, 042401.
77. L. Helseth, T. Fischer and T. Johansen, *Physical review letters*, 2003, **91**, 208302.
78. P. Tierno, S. V. Reddy, T. H. Johansen and T. M. Fischer, *Physical Review E*, 2007, **75**, 041404.
79. P. Tierno, S. V. Reddy, J. Yuan, T. H. Johansen and T. M. Fischer, *The Journal of Physical Chemistry B*, 2007, **111**, 13479-13482.
80. P. Tierno, T. H. Johansen and T. M. Fischer, *Physical review letters*, 2007, **99**, 038303.
81. P. Tierno, R. Golestanian, I. Pagonabarraga and F. Sagués, *Physical Review Letters*, 2008, **101**.
82. A. Soba, P. Tierno, T. M. Fischer and F. Saguès, *Physical Review E*, 2008, **77**, 060401.

View Article Online
DOI: 10.1039/C6LC00707D

83. P. Tierno, T. H. Johansen and F. Sagués, *Physical Review E*, 2009, **80**, 052401.
84. P. Tierno, F. Sagues, T. H. Johansen and T. M. Fischer, *Phys Chem Chem Phys*, 2009, **11**, 9615-9625.
85. P. Tierno, P. Reimann, T. H. Johansen and F. Sagués, *Physical review letters*, 2010, **105**, 230602.
86. P. Tierno, *Physical review letters*, 2012, **109**, 198304.
87. P. Tierno, *Soft Matter*, 2012, **8**, 11443-11446.
88. P. Tierno, T. H. Johansen and T. M. Fischer, *Applied Physics Letters*, 2014, **104**, 174102.
89. A. V. Straube and P. Tierno, *EPL (Europhysics Letters)*, 2013, **103**, 28001.
90. P. Tierno and A. V. Straube, *The European Physical Journal E*, 2016, **39**, 1-7.
91. A. Ehresmann, D. Lengemann, T. Weis, A. Albrecht, J. Langfahl-Klabes, F. Göllner and D. Engel, *Advanced Materials*, 2011, **23**, 5568-5573.
92. D. Holzinger, D. Lengemann, F. Göllner, D. Engel and A. Ehresmann, *Applied Physics Letters*, 2012, **100**, 153504.
93. D. Holzinger, I. Koch, S. Burgard and A. Ehresmann, *ACS nano*, 2015.
94. D. Atkinson, D. A. Allwood, G. Xiong, M. D. Cooke, C. C. Faulkner and R. P. Cowburn, *Nature materials*, 2003, **2**, 85-87.
95. D. A. Allwood, G. Xiong, C. Faulkner, D. Atkinson, D. Petit and R. Cowburn, *Science*, 2005, **309**, 1688-1692.
96. G. Vieira, T. Henighan, A. Chen, A. Hauser, F. Yang, J. Chalmers and R. Sooryakumar, *Physical review letters*, 2009, **103**, 128101.
97. A. Chen, G. Vieira, T. Henighan, M. Howdyshell, J. North, A. Hauser, F. Yang, M. Poirier, C. Jayaprakash and R. Sooryakumar, *Physical review letters*, 2011, **107**, 087206.
98. G. Vieira, A. Chen, T. Henighan, J. Lucy, F. Yang and R. Sooryakumar, *Physical Review B*, 2012, **85**, 174440.
99. M. Prikockis, A. Chen, T. Byvank, G. B. Vieira, B. Peters, F. Yang and R. Sooryakumar, *Magnetics, IEEE Transactions on*, 2014, **50**, 1-6.
100. M. L. Howdyshell, M. Prikockis, S. Lauback, G. B. Vieira, K. Mahajan, J. Winter and R. Sooryakumar, *Magnetics, IEEE Transactions on*, 2014, **50**, 1-7.
101. H. Sohn, M. E. Nowakowski, C.-y. Liang, J. L. Hockel, K. Wetzlar, S. Keller, B. M. McLellan, M. A. Marcus, A. Doran and A. Young, *ACS nano*, 2015.
102. M. T. Bryan, K. H. Smith, M. E. Real, M. Bashir, P. W. Fry, P. Fischer, M.-Y. Im, T. Schrefl, D. A. Allwood and J. W. Haycock, *Magnetics Letters, IEEE*, 2010, **1**, 1500104-1500104.
103. M. Donolato, P. Vavassori, M. Gobbi, M. Deryabina, M. F. Hansen, V. Metlushko, B. Ilic, M. Cantoni, D. Petti and S. Brivio, *Advanced materials*, 2010, **22**, 2706-2710.
104. M. Donolato, A. Torti, N. Kostesha, M. Deryabina, E. Sogne, P. Vavassori, M. F. Hansen and R. Bertacco, *Lab Chip*, 2011, **11**, 2976-2983.
105. M. Donolato, F. Lofink, S. Hankemeier, J. Porro, H. Oepen and P. Vavassori, *Journal of Applied Physics*, 2012, **111**, 07B336.
106. A. Torti, V. Mondiali, A. Cattoni, M. Donolato, E. Albisetti, A. M. Haghiri-Gosnet, P. Vavassori and R. Bertacco, *Appl Phys Lett*, 2012, **101**, 142405.
107. E. Rapoport and G. S. Beach, *Applied Physics Letters*, 2012, **100**, 082401.
108. E. Rapoport, D. Montana and G. Beach, *Lab on a chip*, 2012, **12**, 4433-4440.
109. E. Rapoport and G. S. Beach, *Journal of Applied Physics*, 2012, **111**, 07B310.
110. E. Rapoport and G. S. D. Beach, *Physical Review B*, 2013, **87**.
111. A. Sarella, A. Torti, M. Donolato, M. Pancaldi and P. Vavassori, *Advanced Materials*, 2014, **26**, 2384-2390.
112. G. Nahrwold, J. M. Scholtyssek, S. Motl-Ziegler, O. Albrecht, U. Merkt and G. Meier, *Journal of Applied Physics*, 2010, **108**, 013907.
113. M. A. Akhter, D. J. Mapps, Y. Q. Ma Tan, A. Petford-Long and R. Doole, *Journal of Applied Physics*, 1997, **81**, 4122-4124.
114. J. P. Lazzari, I. Melnick and D. Randet, *Ieee Transactions on Magnetics*, 1967, **MAG3**, 205-&.
115. H. Luo, D. Wang, J. He and Y. Lu, *The Journal of Physical Chemistry B*, 2005, **109**, 1919-1922.
116. M. Nur-E-Alam, M. Vasiliev, V. Kotov and K. Alameh, *Procedia Engineering*, 2014, **76**, 61-73.
117. M. C. Onbasli, L. Beran, M. Zahradnik, M. Kucera, R. Antos, J. Mistrik, G. F. Dionne, M. Veis and C. A. Ross, *Scientific Reports*, 2016, **6**.
118. X. Y. Sun, Q. Du, T. Goto, M. C. Onbasli, D. H. Kim, N. M. Aimon, J. Hu and C. A. Ross, *Acs Photonics*, 2015, **2**, 856-863.
119. T. Boudiar, B. Payet-Gervy, M. F. Blanc-Mignon, J. J. Rousseau, M. Le Berre and H. Joisten, *Journal of Magnetism and Magnetic Materials*, 2004, **284**, 77-85.
120. M. Donolato, B. T. Dalslet and M. F. Hansen, *Biomicrofluidics*, 2012, **6**, 024110.
121. C. Wyatt Shields Iv, C. D. Reyes and G. P. Lopez, *Lab on a Chip*, 2015, **15**, 1230-1249.
122. N. Xia, T. P. Hunt, B. T. Mayers, E. Alsberg, G. M. Whitesides, R. M. Westervelt and D. E. Ingber, *Biomedical Microdevices*, 2006, **8**, 299-308.
123. M. Muluneh, W. Shang and D. Issadore, *Advanced healthcare materials*, 2014, **3**, 1078-1085.
124. J. D. Adams, U. Kim and H. T. Soh, *Proceedings of the National Academy of Sciences*, 2008, **105**, 18165-18170.
125. N. M. Karabacak, P. S. Spuhler, F. Fachin, E. J. Lim, V. Pai, E. Ozkumur, J. M. Martel, N. Kojic, K. Smith and P.-i. Chen, *Nature protocols*, 2014, **9**, 694-710.
126. J. Chung, D. Issadore, A. Ullal, K. Lee, R. Weissleder and H. Lee, *Biomicrofluidics*, 2013, **7**, 054107.
127. H. Lee, A. M. Purdon, V. Chu and R. M. Westervelt, *Nano letters*, 2004, **4**, 995-998.
128. D. Issadore, T. Franke, K. A. Brown, T. P. Hunt and R. M. Westervelt, *Journal of Microelectromechanical Systems*, 2009, **18**, 1220-1225.
129. P. Tseng, J. W. Judy and D. Di Carlo, *Nature methods*, 2012, **9**, 1113-1119.